SUMMARY REPORT
DEVELOPMENT OF AN OPTICAL SUPERHETERODYNE RECEIVER
Period Covered March 1964 - March 1965

Contract No. NAS8-11588

Project Engineer R. F. Lucy

GPO PRICE $ _____

OTS PRICE(S) $ _____

Hard copy (HC) 3.00

Microfiche (MF) .75

Prepared for NASA,
George C. Marshall Space Flight Center
Huntsville, Alabama 35812

17 May 1965

APPLIED RESEARCH LABORATORY
SYLVANIA ELECTRONIC SYSTEMS
A Division of Sylvania Electric Products Inc.
40 SYLVAN ROAD, WALTHAM, MASSACHUSETTS 02154

SUMMARY REPORT
DEVELOPMENT OF AN OPTICAL SUPERHETERODYNE RECEIVER

Period Covered March 1964 - March 1965

Contract No. NAS8-11588

Project Engineer R. F. Lucy

Prepared for NASA,
George C. Marshall Space Flight Center
Huntsville, Alabama 35812

17 May 1965

APPLIED RESEARCH LABORATORY
SYLVANIA ELECTRONIC SYSTEMS
A Division of Sylvania Electric Products Inc.
40 SYLVAN ROAD, WALTHAM, MASSACHUSETTS 02154

ACKNOWLEDGEMENT

This Progress Report was prepared and edited by Mr. Robert Lucy, Project Engineer. Contributors were Dr. C. J. Peters, Mr. K Lang, Mr. E. McGann, Dr. H. Haskal, and Mr. G. Ratcliffe.

ABSTRACT

This report describes the technical investigations performed during the design and development of an optical superheterodyne receiver. The net result of this effort has produced a tested design for a field model system. The ivestigations described include the testing of an experimental over a 6000 foot path, theoptics, photomixing, doppler frequency tracking, optical frequency translation techniques and spatial alignment of the received signal and local oscillator.

TABLE OF CONTENTS

Section		Page
1	INTRODUCTION	1
	1.1 Summary of Progress	1
	1.2 Planned Optical Superheterodyne Receiver Design	2
2	TECHNICAL INVESTIGATIONS	7
	2.1 Sylvania's Experimental Laser System	7
	2.1.1 System Description	7
	2.1.2 Optical and Physical Design	10
	2.1.3 Coherent System Experiments and Performance	11
	2.1.4 System Performance Expectations	18
	2.1.5 Conclusions	22
	2.2 Doppler Frequency Tracking Study	22
	2.2.1 Doppler Shift Considerations	22
	2.2.2 Considerations for Design of Frequency Tracking Loop	28
	2.2.3 Detectors	34
	2.2.4 Local Oscillator	41
	2.3 Optical Tracking	48
	2.3.1 Image Dissector Circuitry	49
	2.3.2 Tracking Tests	51
	2.3.3 Angle Tracking Servo	52

Appendix		
A	COASTING AND SEARCH CONSIDERATIONS FOR FREQUENCY TRACKING LOOP	A-1
B	AN EXPLANATION FOR APPARENT STANDING WAVE PATTERN OBTAINED IN OPTICAL HETERODYNE SYSTEMS	B-1
C	ON MEASUREMENT OF DOPPLER SHIFT WITH LASERS	C-1
D	NOISE FIGURE FOR PHOTOTUBES	D-1
E	SPATIAL TRACKER SERVO CONTROL DESIGN	E-1

LIST OF ILLUSTRATIONS

Figure		Page
1	Receiver Van	4
2	Optical Superheterodyne Receiver	5
3	Block Diagram of Laser System	8
4	Photo of Van Interior	9
5	Optical Layout of Laser System	12
6	Receiver Optics Physical Design	13
7	Oscillogram of Return Signal	16
8	RF Mixer Output Versus Doppler Shift Frequency	27
9	Translated Doppler Frequency Curve	29
10	AFC Loop Block Diagram	30
11	Optical Superheterodyne Receiver Noise Figure	39
12	Optical Superheterodyne Noise Figure Using TWP With TSEM Amplification	40
13	Frequency Translator Using Two Plane Modulators In Tandem	44
14	Frequency Translator Photo	45
15	Sweep and Signal Processing Circuitry	50
A-1	A Missile Tracking System	A-3
A-2	Search Region for Frequency Loop	A-3
A-3	Frequency Search Pattern	A-3
B-1	Block Diagram of an Optical Superheterodyne System	B-2
B-2	Laser Spectrum (text)	B-6
B-3	Amplitude Versus Range Curve	B-7
C-1	A Doppler Laser System	C-2
C-2	Spectrum of Subcarrier Doppler Terms	C-2
C-3	Spectrum of Laser Beats	C-2

LIST OF ILLUSTRATIONS - continued

Figure		Page
E-1	Postulated Operational Environment	E-1
E-2	Block Diagram of Control Loop	E-3
E-3	Log Magnitude Plot of Rate Loop Gain Transfer Function	E-6
E-4	Image Dissector Output Waveforms with Star Scan Pattern as Indicated	E-6

SECTION 1

INTRODUCTION

1.1 SUMMARY OF PROGRESS

Under this program we have demonstrated the feasibility of operation of an optical superheterodyne receiver with large diameter optics in the atmosphere. Such a receiver has been operated over a one-mile atmospheric path. The results of this experiment indicate that sufficient coherence of the beam will be retained for both horizontal and vertical paths through the atmosphere to make operation of the optical superheterodyne possible and hence make it possible to realize the advantages of the optical superheterodyne receiver. As a result of the experiments and accompanying studies a design for a deliverable model of an optical superheterodyne receiver has been achieved. This unit is to be constructed in the coming months.

A major accomplishment of this first year's program has been the experimental confirmation of an optical design which preserves coherence of the received optical beam and which also expands the allowable angular tracking error. Assuming that both the received signal and local oscillator are plane waves the allowable tracking error for an optical superheterodyne receiver with an optical aperture on the order of 8 inches would be in the microradians. Our optical design expanded this allowable tracking error to approximately 200 microradians. This means that an angular tracking servo of comparatively conventional design can be used to track the incoming signal.

In the original proposal it was stated that the main tracking servo would track a target to an accuracy of 1 milliradian, and the necessary collimation between the received signal and the local oscillator would be attained by means of a vernier servo. As a result of the optical design work, these requirements have been relaxed so that the vernier servo can be eliminated and adequate tracking obtained by tightening up the tolerance on the main tracking servo. Elimination of the vernier servo greatly simplifies the system design, improves the reliability, and simplifies the initial acquisition of the signal. The higher performance required of the main tracking servo can still be achieved with conventional components.

The problems encountered in developing an automatically tuned receiver for doppler frequency tracking have been studied. A receiver which can cover a 1 Gc/s doppler range appears to be feasible with presently available components.

We have demonstrated that electro-optic frequency translators can be used to derive the local oscillator signal. These frequency translators, in conjunction with wide bandwidth detectors, will make it possible to handle 20 Gc doppler shifts in the future. This particular work was supported under the Company Research Program but derived its motivation from the optical superheterodyne project.

Various photodetectors including PIN diodes, photomultipliers and traveling-wave photodetectors have been evaluated for this receiver. The present choice is to use a wide bandwidth photomultiplier. Crossed field photomulitpliers offer promise for future receivers.

In this project we have also generated performance specifications for gas lasers to be used in communication-like systems.

These specifications are primarily concerned with the noise output of the laser and the frequency content of the laser.

In a company research program we have demonstrated the transmission of an amplitude modulated video bandwidth signal through the atmosphere. This accomplishment is a necessary adjunct to the demonstration of the operation of the optical superheterodyne receiver.

The detailed results of the technical investigations are reported in Section 2 of this report. The recommended design for a deliverable model of an optical superheterodyne receiver based upon these investigations is presented in Section 1.2.

1.2 PLANNED OPTICAL SUPERHETERODYNE RECEIVER DESIGN

The design phase for the optical superheterodyne receiver is substantially completed. In the next phase of the optical superheterodyne project, we intend to construct an operational model of the optical superheterodyne receiver. This optical superheterodyne receiver will be suitable for conducting detailed scientific propagation experiments, tracking experiments,

and communications experiments. Sufficient versatility will be built into the receiver to permit reception of amplitude-modulated video bandwidth signals and amplitude- and frequency-modulated audio signals. Bandwidth of the receiver will be controllable to permit optimization of the receiver for the experiment at hand. The servo systems will be adequate to permit tracking of a transmitter mounted on a vehicle traveling at velocities up to 1000 feet per second and undergoing accelerations up to 100 ft/s^2 at a minimum range of 5000 feet.

This receiver will be installed in a van similar to that shown in Figure 1. The van mounting makes it comparatively easy to perform experiments at various geographical locations and also provides a much larger field of view than is usually available from a laboratory building.

The block diagram for the optical superheterodyne receiver is shown in Figure 2. Generally speaking, the operation of the diagram is self-explanatory. The detailed specification for each of the blocks shown here has been generated during the design phase of this project. It should be noted that a double heterodyne system is used for this receiver. Here the local oscillator laser is stabilized and operates at an offset frequency to allow satisfactory operation at zero doppler shift. The output frequency from the photomixer, where the incoming optical signal is heterodyned with the local oscillator signal, will lie in the frequency range of $\pm$ 500 Mc. The second heterodyne step produces the relatively low frequency intermediate frequency. Doppler frequency tracking is provided by an AFC loop that controls the RF local oscillator input to the RF mixer.

An alternate design would use a single heterodyne system. This system would perform the frequency tracking function by tuning an optical local oscillator and eliminating a tunable RF local oscillator. This system which would seem to be easier was not considered because at this writing the performance and stability of single frequency lasers were not known. If during our future investigations we find the optical local oscillator suitable for this application then a single heterodyne system would probably be implemented in place of the one described. The single heterodyne system would be less complicated, more desirable, and still provide the flexibility to extend the system to 20 Gc/s coverage by use of frequency translator techniques.

Figure 1. Receiver Van.

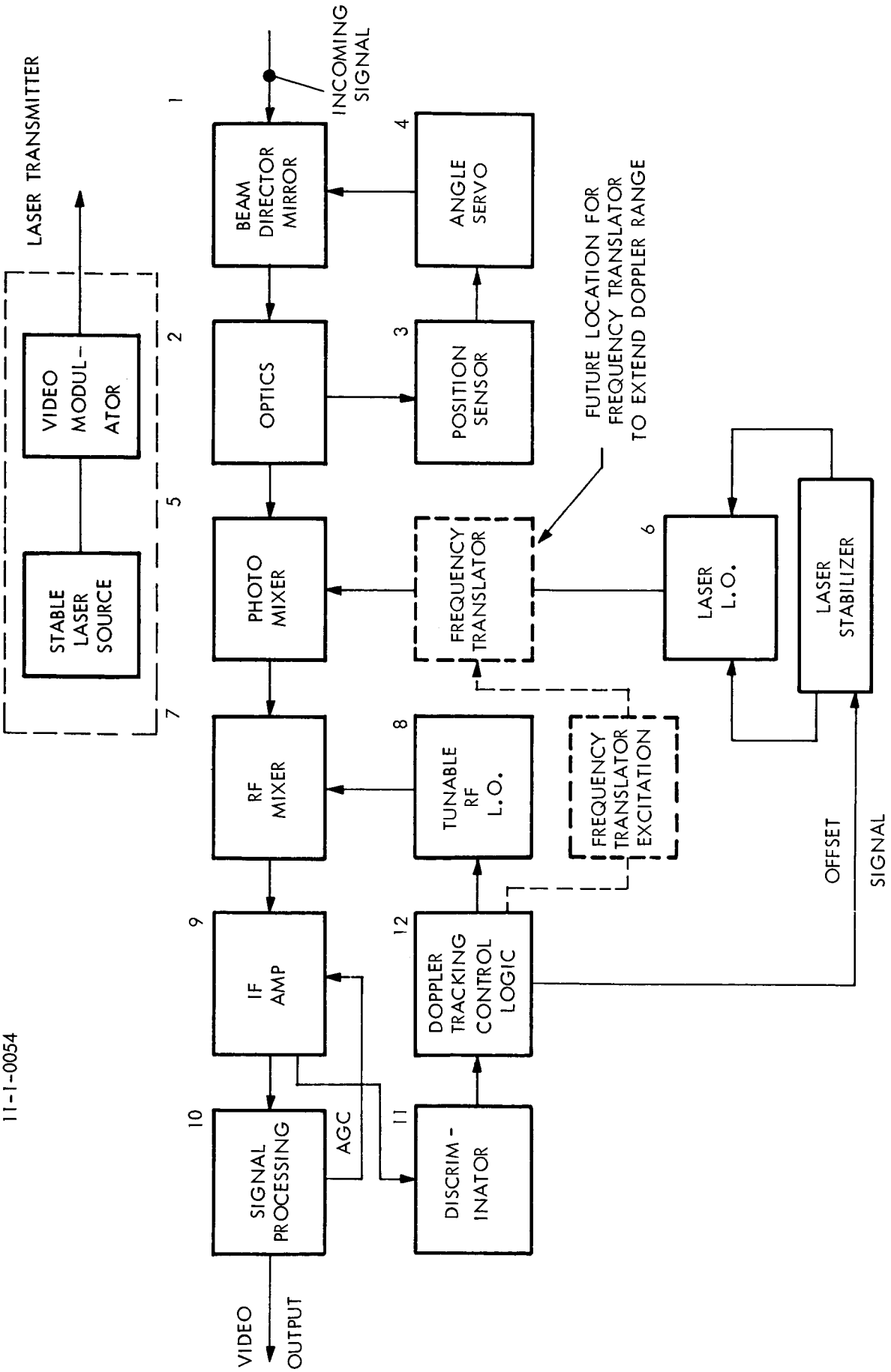

Figure 2. Optical Superheterodyne Receiver.

Recent preliminary tests with single frequency lasers in our laboratory now appear to favor the single heterodyne system.

SECTION 2

TECHNICAL INVESTIGATIONS

2.1 SYLVANIA'S EXPERIMENTAL LASER SYSTEM

2.1.1 System Description

Prior to the start of Contract No. NAS8-11588 Sylvania's Applied Research Laboratory had been actively engaged in the study and development of coherent laser systems. As a result of the company sponsored effort a first model of an optical superheterodyne receiver with large collecting optics which operated over a 1200 foot atmospheric path had been constructed. The success of this receiver led to the design and construction of a coherent laser tracking system mounted in a mobile van unit. This system has been used as an experimental model to aid in the development of a design for an optical superheterodyne receiver under Contract No. NAS8-11588.

The coherent laser tracking system consists of an optical superheterodyne receiver, gas laser transmitter, and tracking servo to direct the beam as shown in Figure 3. The van installation is shown in Figures 1 and 4.

The output from a helium-neon gas laser operating at 6328Å is directed via a mirror through the atmosphere to a distant retroreflector. The retroreflector return is reflected by the beam director mirror into the collecting optical system. The optical system consists of a primary 8-inch diameter parabolic mirror and a secondary collimation mirror. This system reduces the size of the return signal and forms a beam to be mixed with the optical local oscillator signal. One gas laser produces both the transmitted beam and the local oscillator signal. A frequency offset for the local oscillator signal is generated by the frequency translator. The system makes use of the spatial and temporal coherence of the gas laser output. Thus, in the optical system care has been taken to design and maintain optical component tolerances to within a few percent of a wavelength over the spatial extent of either the transmitted, received, or local oscillator beams. Mechanical tolerances are extremely important in the optical heterodyne portion of the system. Both the received signal and local

11-1-0055

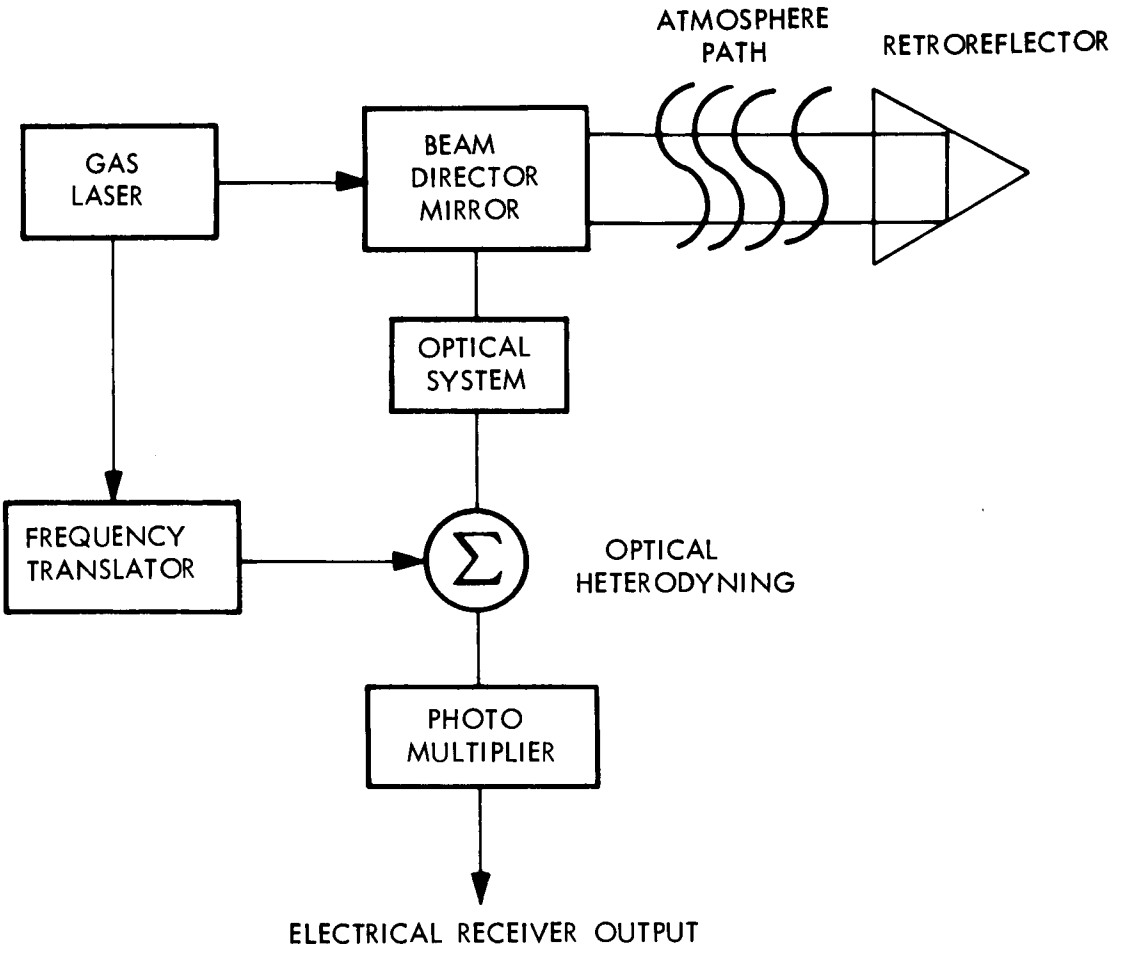

Figure 3. Block Diagram of Laser System.

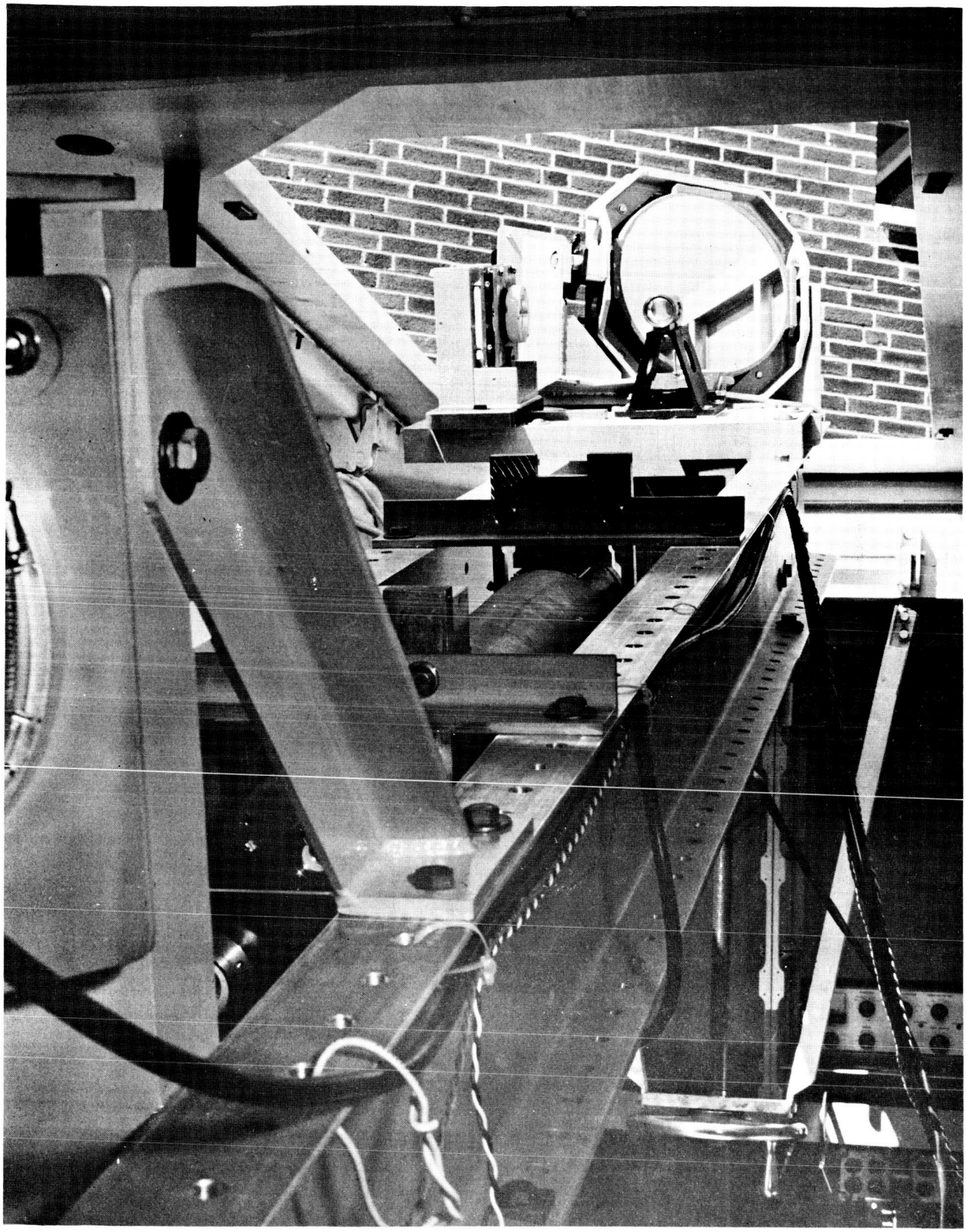

Figure 4. Photo of Van Interior.

oscillator signal phase fronts are aligned to within a fraction of a wavelength within the system. The gas laser discharge tube has been mounted in a rugged nonmicrophonic cavity which is insensitive to acoustical and short-term temperature disturbances, thus providing extreme frequency stability.

The tolerances in optical heterodyne systems are usually discussed in terms of the angular misalignment between a received signal and the local oscillator signal. Alignment requires at least half-wave spatial matching of the two beams for reasonable performance. Thus, if the beams both are 1 cm in linear dimension an angular misalignment of about 32 microradians corresponds to a half-wave misalignment at 6328Å. In our system the collected optical signal is reduced in size by the ratio of the secondary to primary mirror focal lengths in order to perform the mixing operation at reduced sizes. Angular misalignments due to an angular deviation at the primary mirror is thus magnified. If we were merely mixing collimated beams, angular perturbations produced by the atmosphere on the return beam, angular jitter of the tracking mount, or vibration of the system would exclude any form of operation. This problem is solved by the unique design of the system. In Sylvania's system, mixing is performed by first establishing very precisely an effective common source point for both the return beam and the local oscillator beam. The beams are then allowed to diverge at the same rate and thus have the same size at the photomixer. To the first order, angular misalignments caused by variations in angle of arrival merely produce an area mismatch. That is, the two spherical waves at the mixer retain the same apparent common center and only the area of overlap changes. This concept has yet to be rigorously proved, however, actual operation of the system in the field mounted in a mobile van provides evidence of system operation which supports this concept.

2.1.2 Optical and Physical Design

The prototype model used for optical heterodyne experiments was a second generation model. The original model optics design was described in the document "Proposal for Development of An Optical Superheterodyne Receiver" 22 November 1963, submitted to NASA by Applied Research Laboratory, Sylvania Electronic Systems, 40 Sylvan Rd., Waltham, Mass. As a result

of tests on this original design the optics and physical design used in the van mounted model were developed. This design was discussed in detail in a subsequent report.[1]

The trace of signal rays and local oscillator rays through the system is shown in Figure 5. The output of the laser is reflected by mirrors to the beam director mirror and thence toward the distant retroreflector. The return rays are reflected from the beam director to the parabolic mirror and thence to the secondary beam forming mirror. The collimated return signal is then mixed with the local signal at the mirror adder and the resultant beat detected by the photomultiplier. The local oscillator signal originates at the laser but has been shifted in frequency by the frequency translator to provide a frequency offset. The laser local oscillator signal is focused by a beam forming lens. The object of the lens is to form a local oscillator beam which has a focus point corresponding to the focus point of the secondary mirror. This matching reduces its sensitivity to angular mismatch.

Another signal takeoff at C provides the optical error signal for the angle tracking servo. A spotting telescope is also incorporated in the system for visual data takeoff.

These optics were found to be satisfactory for use in the optical superheterodyne receiver design.

The physical design of the optical portion of the receiver is shown in Figure 6. This drawing shows the main signal collecting optics, the various alignment fixtures, and the viewing telescope. The angle tracking servo, which fits on the right end of the optical structure, is not shown.

2.1.3 Coherent System Experiments and Performance

Coherent light propagation experiments over 6,000-foot atmospheric paths have been performed. They were carried out with the coherent laser tracking system which uses an optical superheterodyne receiver. The object of the experiments has been to determine the effects of the atmosphere on the heterodyne frequency signal. Amplitude, phase, and angle of arrival fluctuations all produce signal variations. The equipment, mounted in a

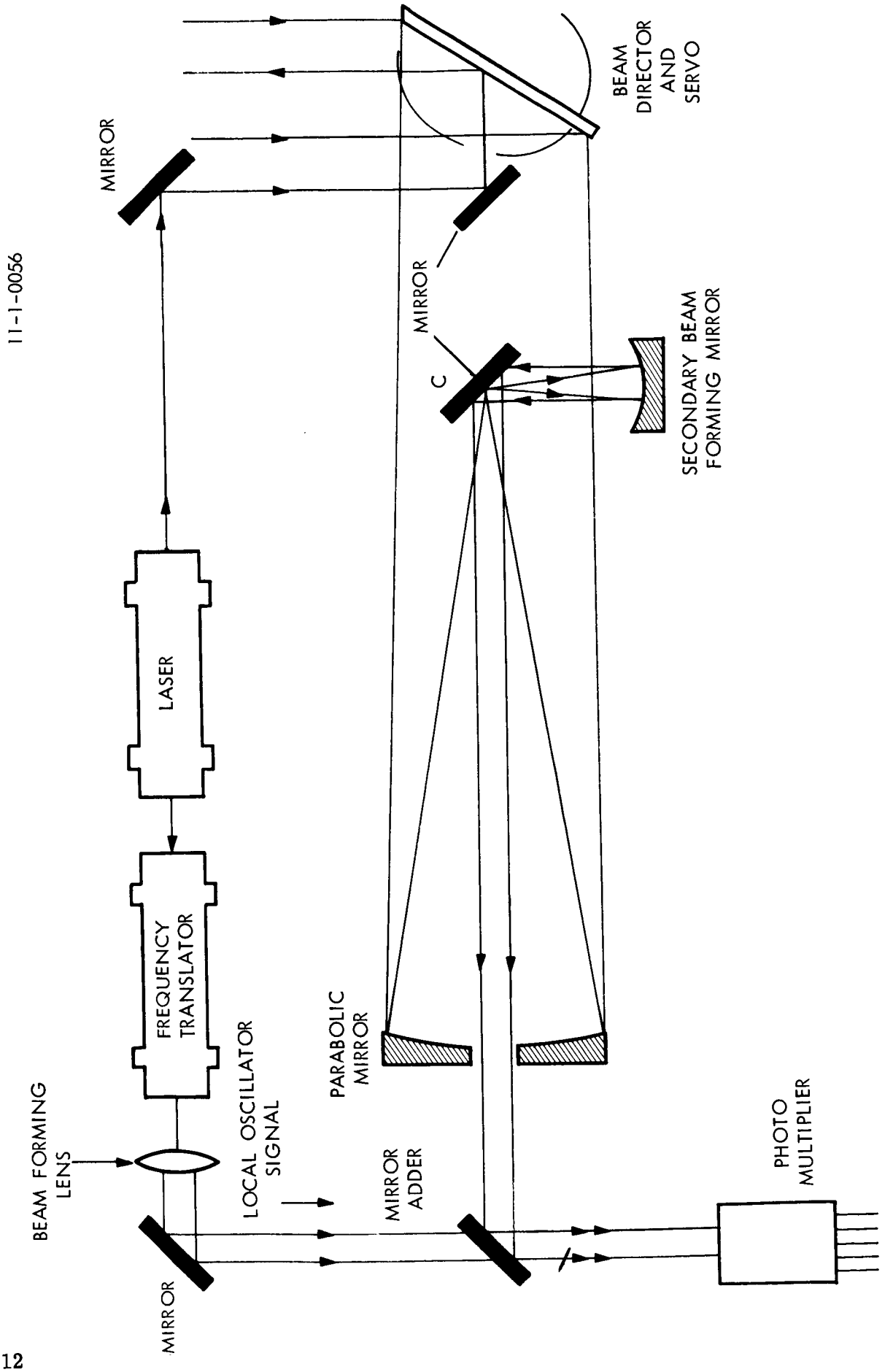

Figure 5. Optical Layout of Laser System.

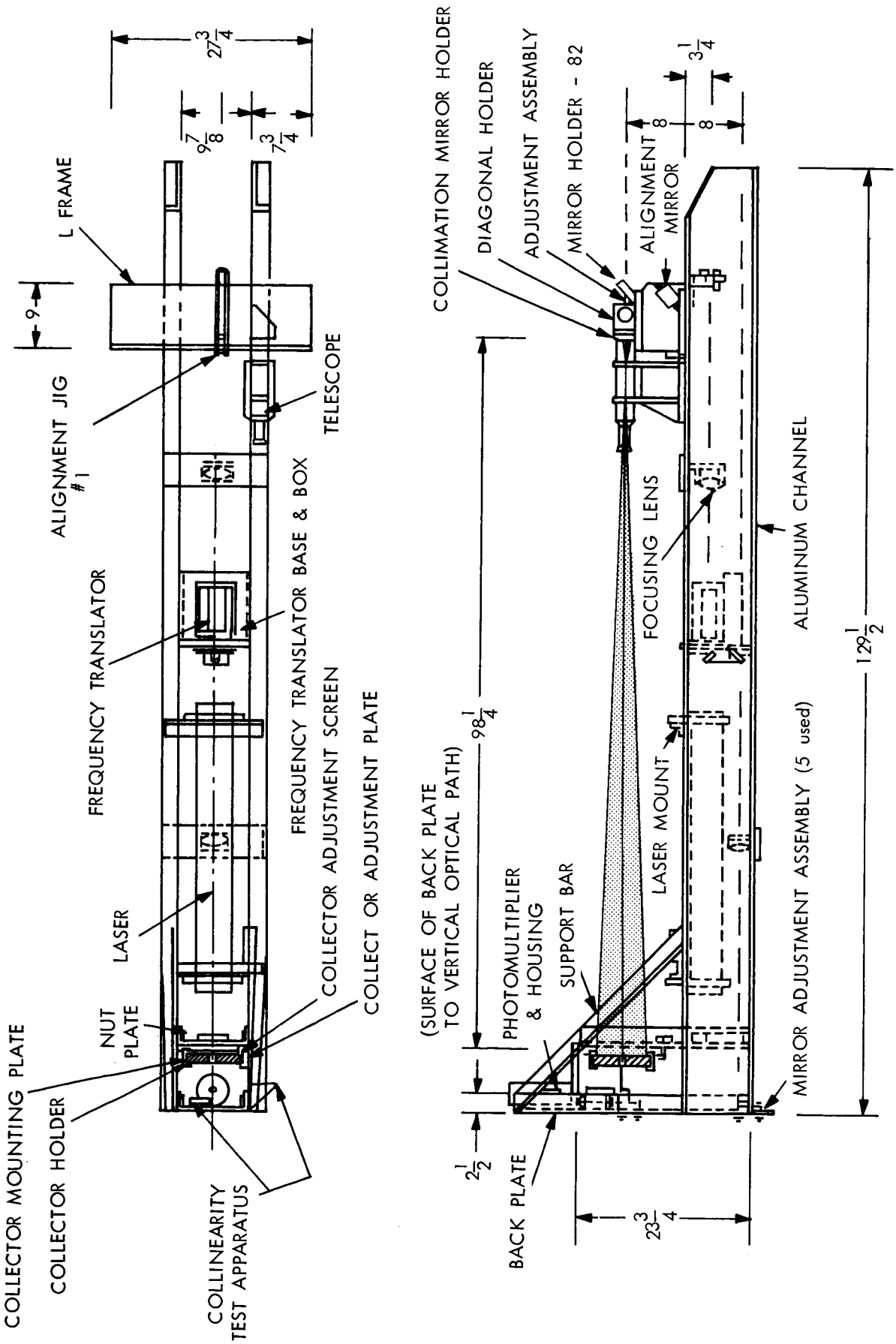

Figure 6. Receiver Optics Physical Design.

mobile van is shown in Figure 4. A block diagram of the system is shown in Figure 3. Data has been taken over the 6,000-foot atmospheric path under varying meteorological conditions. The transmitter-receiver has been located at the Sylvania Waltham Laboratories, and the retroreflector is located on Bear Hill which is 3000 feet away. The elevation of the transmitter-receiver and retroreflector installation are approximately the same. The terrain in between is a tree studded valley whose elevation is approximately 100 feet less than the propagation path. Typical system performance data is summarized in Table I.

TABLE I

COHERENT LASER SYSTEM DATA

Radiated Power	5×10^{-4} watt
Radiated Beamwidth (5%)	5×10^{-4} radian
Average* Received Signal Power	3.2×10^{-6} watt
Average* Signal Power at Photomixer	1.3×10^{-6} watt
Local Oscillator Power	1.8×10^{-6} watt
Peak Local Oscillator Signal to Noise	42 dB
Average* Beat Frequency Signal to Noise	38 dB
Heterodyne Efficiency**	-10 dB

*Average value signal fluctuating because of atmospheric propagation effects.

**Ratio of average heterodyne signal level to maximum theoretical beat signal level corresponding to measure values of average received signal and local oscillator signal.

Typical signal returns are shown in the oscillogram, Figure 7. This record was obtained in June 1964 on a fair weather day. The wind velocity was about 20 miles per hour. The 5% laser beamwidth at the 2.5-inch diameter retroreflector was about 3 feet. The top trace shows the beats generated by heterodyning the return with the local oscillator. The beats occur in groups because of the manner in which the local oscillator frequency offset was obtained and should repeat every 1.7 ms. The rounding of the envelope is due to the amplifier bandwidth. The signal was filtered by a bandpass filter which passed 3 kc to 10 kc to remove the low-frequency intensity fluctuations. Frequency translation was performed mechanically. The laser output was shifted in frequency to form the local oscillator signal by reflecting the beam from a moving mirror. Since a reciprocating mirror motion was actually used, the doppler frequency shift varied with time giving rise to the envelope of the waveform in Figure 7. The lower trace in Figure 7 is the return signal passed through a low-pass filter with a cutoff frequency of 1 kc. No beats are present because they do not fall within this bandwidth. The trace is a representation of this instantaneous photocurrent. It indicates the signal power fluctuations since the atmospheric turbulence produces only low-frequency variations. Approximately 80-90 percent amplitude modulation is represented by intensity signal excursion. In general one would expect the beat signal to be somewhat smoothed as compared with the optical power fluctuation since the beat signal is proportional to the square root of the received optical power. Preliminary tests indicate this to be true at times although other effects can be observed.

In our preliminary observations we have noted pronounced beat amplitude variations that cannot be correlated with the amplitude fluctuations. These observations as shown in Figure 7 include increases in beat amplitude with decreasing optical power return and vice versa. Also complete beat signal dropouts without intensity dropouts have been observed. In Figure 7 the largest beat signal occurs at a medium intensity level; smaller beat then occurs at a higher intensity level, and a partial dropout has occurred between these beats. The fourth beat is also missing. Then when the power is low a relatively good beat occurs. The low amplitude fine structure in the beat signal display is laser local oscillator noise.

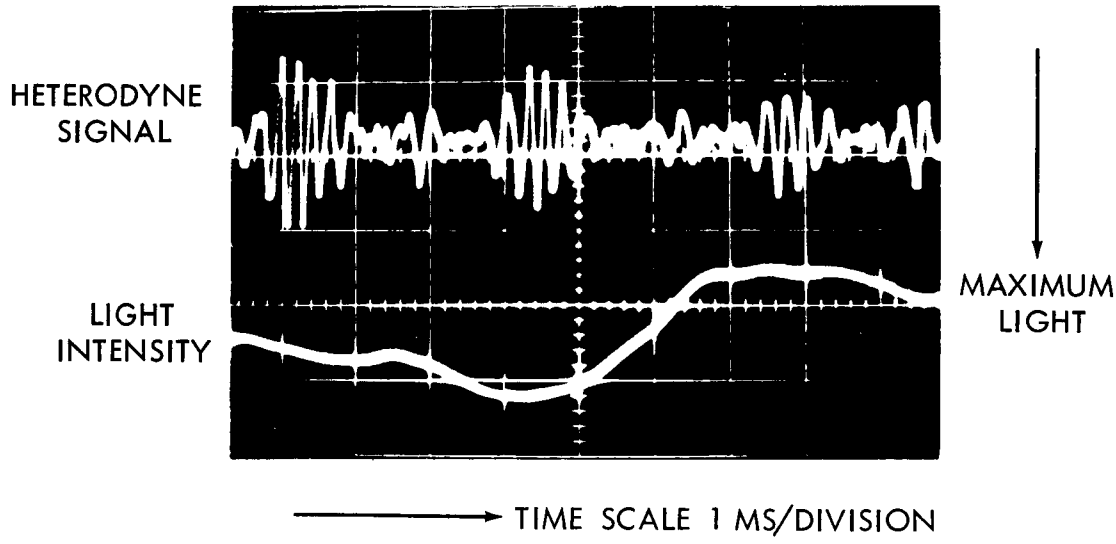

Figure 7. Oscillogram of Return Signal.

The additional modulation on the beat signal can be produced by two different effects or a combination of these effects. One could be phase fluctuations across the returning beam introduced by the atmosphere and the other could be fluctuations in the angle of arrival which produces a misalignment in the heterodyning signals.

Attempts have been made to operate the superheterodyne system to the retroreflector on the TV tower 7 miles away. Upon increasing the range from 6000 feet to 14 miles we found the noncoherent signal losses increased by about a factor of 4 to 6 times that loss anticipated by the normal beam divergence effects. This additional loss has been attributed to haze scattering and attenuation. Visual observations made on the return signal have shown that the size of the return approximates the expected 5 inch diameter return from the 2.5 inch diameter retroreflector. Thus the beam has not seriously deteriorated over this range under the propagation conditions. During the tests to the TV tower a 0.2 milliradian beamwidth was used. Line of sight angular fluctuations of the beam was approximately less than 0.1 milliradian.

In three tests we were unable to achieve coherent operation. The instability of the local oscillator noise has proven to be the most severe limitation. This noise is apparently produced by longitudinal mode pulling in the laser. The resultant interbeating between modes produces a continually changing noise spectra as the modes apparently change their relative frequency separation. This noise is sensitive to the laser cavity adjustment. A minimum noise level can be obtained in the hemispherical cavity by precise adjustment of the mirror separation and alignment with the amplifying gas column. At best we were able to adjust the cavity such that a minimum but somewhat unstable cyclic noise is observed. The noise amplitude varies in time from approximately the expected photon induced shot noise level to noise composed of sine waves at many different frequencies that are continually changing. The repetition rate is associated with the slow thermal drift of the cavity. The amplitude-frequency characteristic of this noise is approximately a $\frac{1}{f}$ distribution. In the frequency range of operation (4-10 kc as determined by the present local oscillator offset) the maximum amplitude of this noise at the best cavity adjustment is

approximately 20 to 40 times the minimum. The noise cycles from the minimum shot noise level through a continually varying frequency sine wave, thence into a multifrequency sine wave spectra, then back to the varying sine wave and finally returning to the shot noise level. The shot noise level during these tests lasted only about 10 seconds. It is during this low-noise period that beat signals were searched for on the TV tower range. It was not possible to perform fine system adjustments during this short period. When operating on the 3000 foot range this problem is overcome by the high signal-to-noise ratio. During the tests the beamwidth was adjusted to a minimum size compatible with atmospheric turbulence as discussed above. In each test a noncoherent return was measurable. Calculations indicated that ideally a 10:1 beat signal to shot noise level should be observable.

The best way to alleviate this difficulty is to substitute a single longitudinal mode laser for the present multimode laser. Because of the noise problem the long-range shot has not been given a fair trial and the results to date are inconclusive.

2.1.4 System Performance Expectations

2.1.4.1 Range Equation

The received signal power P_s at the photomixer is given by the expression

$$P_s = \frac{\epsilon_1 P_T A_c}{\Omega_T R^2} \tag{1}$$

where

ϵ_1 = receiver optics efficiency

P_T = transmitter power

A_c = optical collector area

Ω_T = transmitter beamwidth

R = distance between stations.

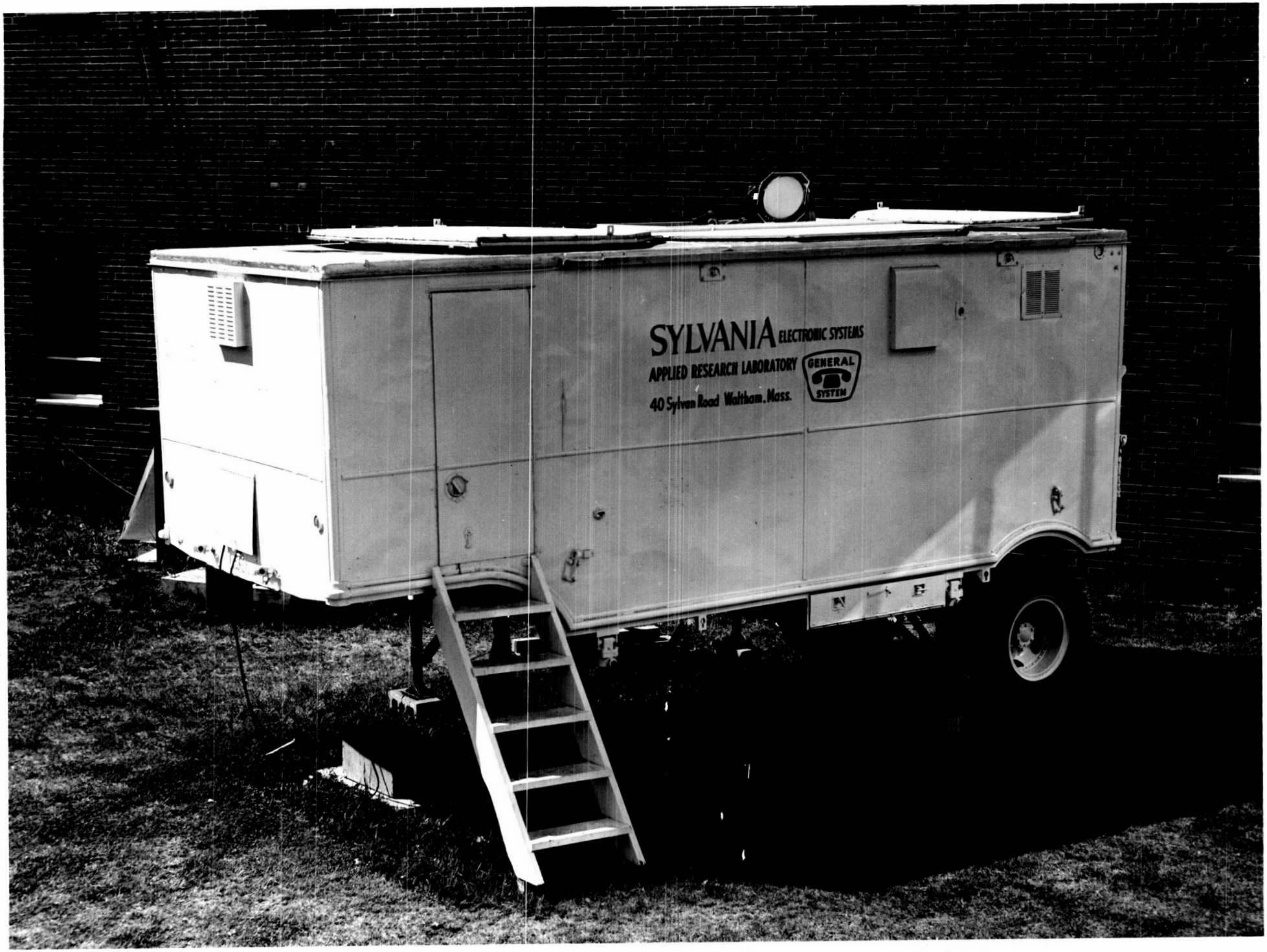

SYLVANIA ELECTRONIC SYSTEMS
Government Systems Management
for GENERAL TELEPHONE & ELECTRONICS

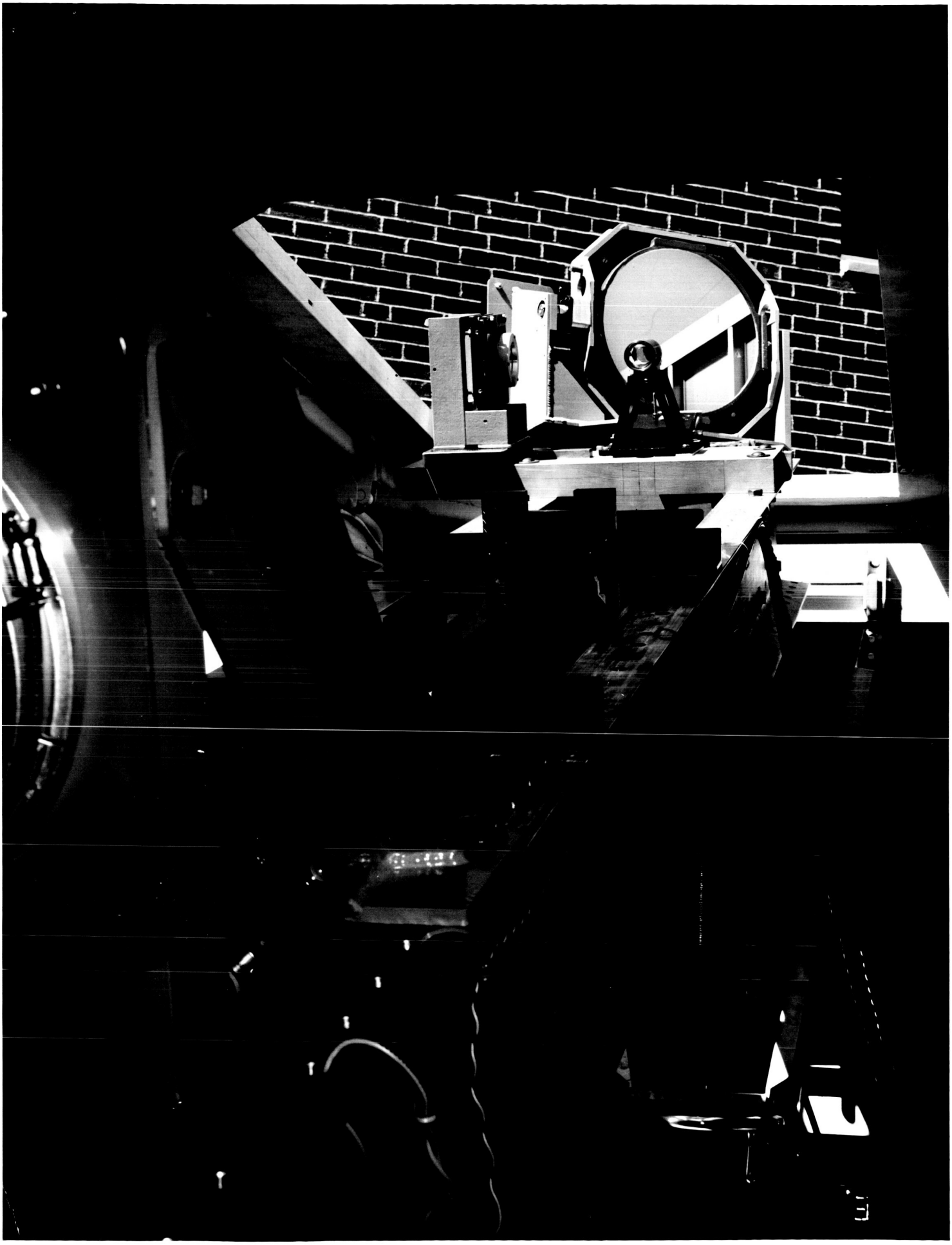

The heterodyne receiver will operate in the photon noise-limited operation mode; thus, the voltage signal-to-noise ratio N is given as

$$N = \epsilon_2 \sqrt{\frac{P_s Q}{h\nu \Delta f}} \tag{2}$$

where

ϵ_2 = receiver heterodyne efficiency

Q = photomixer quantum efficiency

$h\nu$ = energy per photon

Δf = receiver electrical bandwidth.

The collector area may be written as

$$A_c = \frac{\pi}{4} D_c^2 \tag{3}$$

where D_c is the collector diameter. The beamwidth θ_T in radians is related to Ω by the expression

$$\Omega_T = \frac{\pi}{4} \theta_T^2 \ . \tag{4}$$

Substituting Eqs. (3) and (4) in Eq. (1) then substituting the resultant equation in (2) and solving for R gives the range equation

$$R = \frac{\epsilon_2 D_c}{N\theta_T} \sqrt{\frac{\epsilon_1 P_T Q}{h\nu \Delta f}} \ . \tag{5}$$

2.1.4.2 Separate Transmitter-Receiver Stations

The range for the separate receiver-transmitter stations may be determined by using typical values found with the present experimental systems and the transmitter estimates. From experience we estimate a good signal-to-noise voltage ratio is 10:1. The other parameters are

$P_T = 10^{-4}$ watt

$\theta = 4.5 \times 10^{-4}$ radian

$\epsilon_2 = 0.3$

$D_c = 0.2$ m

$\epsilon_1 = 0.5$

$Q = 5 \times 10^{-2}$

$h\nu = 3.1 \times 10^{-19}$ joule

$\Delta f = 4$ Mc

for which R = 19 kilometers (12 miles).

2.1.4.3 Retroreflector Case

When a retroreflector is the target, the difference between that case and the previous case is that the range is reduced by the ratio of the retroreflector diameter to collecting optics diameter; providing the optics diameter is greater than twice the retroreflector diameter. Using a 2 1/2 inch diameter retroreflector and since the optics diameter is 8 inches, the range is reduced by a factor 3:1. The range then becomes 6 kilometers or 3 3/4 miles. This provides for a total atmospheric transmission path for evaluation of 7 1/2 miles. A greater range and, hence, more margin for error in this estimate is desirable, especially when considering the signal-to-noise dynamic range required in the AGC circuitry. However, we believe with careful design the demonstration experiments can be performed satisfactorily.

2.1.4.4 Servo Tracking System Sensitivity

In the servo tracker noncoherent detection is used. This form of detection is possible because even in the presence of severe background radiation the cumulative effects of narrow optical bandwidth, narrow field of view and a narrow electrical bandwidth allow operation in a noncoherent mode. To show this, the power reflected by a sunlit cloud in a 10 Å band for a 1 milliradian field of view and collected by 8-inch diameter optics is (using Eq. (48) and Table II from Reference 2):

$$P_B = 7.5 \times 10^{-9} \text{ watt} .$$

Using Eq. (1) for the retroreflector case and since the value of ϵ_1 is 3×10^{-2}; i.e., in the position signal pickoff we have allowed 10 percent for this function, the transmission of 10 Å filter is 30 percent thus ϵ_1 is 3×10^{-2}, the value of P_s is given by

$$P_s = 1.65 \times 10^{-9} \text{ watt} .$$

The signal-to-noise ratio for the noncoherent case is

$$N = \sqrt{\frac{P_s^2 Q}{2h\nu\Delta f\left(P_s + P_B\right)}} . \tag{6}$$

We are interested primarily in the value of N in order to determine the tracking accuracies obtainable. Solving Eqs. (1), (2), and (3) as before and substituting for P_s in Eq. (6) gives an expression that may be written as

$$N = \frac{D_c}{R\theta}\sqrt{\frac{Q\epsilon_1 P_T}{2h\nu\Delta f}\left(\frac{1}{1 + P_B/P_s}\right)} . \tag{7}$$

(This form is used to show the effect of background in reducing N.) The values for substitution are for the retroreflector case:

$$D_c = 6.25 \times 10^{-2} \text{m}$$

$$R = 6 \times 10^{3} \text{m}$$

$$\theta = 4.5 \times 10^{-4} \text{radian}$$

$$Q = 5 \times 10^{-2}$$

$$\epsilon_1 = 7 \times 10^{-2}$$

$$P_T = 10^{-4} \text{watt}$$

$h\nu = 3.1 \times 10^{-19}$ joule

$\Delta f = 10$ c/s.

The calculated value of N is 2500 which will be adequate for tracking since the accuracy required is about 0.1 mr out of less than 1 mr.

2.1.5 Conclusions

In the experimental program described in this section we have both tested and developed a suitable wide aperture optical system for an optical superheterodyne receiver. Operation of this system in the field under a variety of real atmospheric conditions has led us to the following conclusions:

1) Coherent laser systems are practical and can be operated with reasonable efficiency over long atmospheric paths.

2) Coherent systems behave in a predictable manner.

3) System design and performance will be limited by atmospheric propagation effects.

4) There is insufficient atmospheric data and experiments to design an optimum coherent system for particular applications.

5) There is a need for further technique work to mimimize the effects of the atmosphere on system performance.

2.2 DOPPLER FREQUENCY TRACKING STUDY

2.2.1 Doppler Shift Considerations

Relative motion between a transmitter and receiver or relative motion between a transmitter-receiver combination and a retroreflector will produce a doppler frequency shift. At optical frequencies this corresponds to a frequency shift of about 1 Mc/s for a vector velocity of one foot per second. In an extreme case where two satellites are traveling in opposite directions the relative velocity could be as high as 10 miles/second. This corresponds to a doppler shift of 50 Gc/s. Considering that in a superheterodyne receiver the beat frequency between the desired signal and the local oscillator must fall within the bandwidth of the narrowest intermediate frequency amplifier, an automatically tuned receiver is required. For maximum

sensitivity the bandwidth of the final IF amplifier is the information bandwidth required for the system. For high quality standard television this bandwidth ϕ is 10 Mc/s. This bandwidth with a doppler frequency coverage of 20 Gc/s is the ultimate goal for a superheterodyne receiver useful in space communications.

Important considerations for the development of a sensitive receiver include the detector, optical local oscillator, frequency translator, and frequency tracking.

When there is no relative motion between the receiver and transmitter there will be no doppler shift. If both the laser local oscillator and laser transmitter are at the same frequency, the output of the photodetector will be signal modulation. In order to utilize the advantages of intermediate frequency amplification an offset between the local oscillator and received signal is necessary. Consider the laser transmitter to be at a frequency f_L and the local oscillator of the receiver to be at $f_L + f_T$ where f_T is the frequency translation. The photomixer frequency response at the difference frequency f_{PM} given by the relation

$$(f_{PM})_c = \left| \left(f_L + f_T\right) - \left(f_L + f_D\right) \right| \tag{8}$$

$$= \left| \left(f_T - f_D\right) \right| \tag{9}$$

for the closing case, and

$$(f_{PM})_r = \left| \left(f_L + f_T\right) - \left(f_L - f_D\right) \right| \tag{10}$$

$$= \left| \left(f_T + f_D\right) \right| \tag{11}$$

for the receding case, where f_D is the doppler shift due to the relative velocity between the transmitter and the receiver. For a downward frequency translation the closing and receding cases are interchanged.

If continuously variable optical frequency translation were used then the value of f_T in Eqs. (9) and (11) would have to be controlled to keep $(f_{PM})_c$ or $(f_{PM})_r$ at the frequency of the following IF amplifier. Investiga-

tions of wideband optical frequency translators over several Gc/s indicate that because of the power requirements imposed by the associated wideband electrical modulator it is presently more practical to consider optical frequency translators only for fixed offsets and not as a means of providing a continuously variable optical source. It was thus concluded that to provide continuous doppler tracking a tunable laser or a second frequency conversion* using a variable RF local oscillator would be preferred. It was also concluded that optical frequency translation using electro-optic modulation techniques can be utilized best for a fixed translation. The fixed frequency offsets would be used in a bandswitched receiver where bandswitching is required to place the doppler shifted optical beat frequency within the photomixer bandwidth. Furthermore because of the lack of a tunable stable laser local oscillator, doppler frequency tracking in an automatically tuned RF receiver is preferred at preset. When an RF mixer follows the optical mixer the mixed frequency outputs f_m are

$$f_m = f_{lo} \pm f_{PM} \tag{12}$$

where f_{lo} is the RF local oscillator frequency. In order to get a maximum useful range of f_{PM} and to avoid ambiguities the difference frequency is chosen as the desired IF frequency, and the local oscillator is made larger than f_{PM}. The undesired outputs of the mixer are the sum or image frequency, the local oscillator and the photomixer output. If any of these signals enter the IF amplifier they represent false signals that must be rejected in order to eliminate ambiguities in the frequency tracking. The easiest way to avoid this complication is to require that these frequencies never enter the IF amplifier. These requirements are

$$f_{image} \geq f_{i\text{-}f} + \Delta f_{i\text{-}f} \tag{13}$$

$$f_{lo} \geq f_{i\text{-}f} + \frac{\Delta f_{i\text{-}f}}{2} \tag{14}$$

$$f_{PM} \geq f_{i\text{-}f} + \Delta f_{i\text{-}f} \,. \tag{15}$$

*See footnote on page 3.

The difference in the lower limits on f_{PM} and f_{image} as compared to f_{lo} are due to the modulation sidebands present on f_{image} and f_{PM}. Since the image frequency and the local oscillator frequency are greater than the photomultiplier output signal, Eq. (15) represents the principal requirement. The minimum allowed value of f_{PM} is

$$(f_{PM})_{min} = f_{i-f} + \Delta f_{i-f} \quad . \tag{16}$$

The direction of frequency translation was selected to be upward for this analysis. Thus, with increasing doppler the photomultiplier output increases in frequency for the receding case and decreases in frequency for the approaching case as shown in Eqs. (9) and (11). Consequently, the receding case is limited by the photomultiplier upper bandwidth cutoff and the closing case is limited by the selection of the IF amplifier. This situation would be reversed if a downward frequency translation were chosen.

The equations for the local oscillator frequency are

$$(f_{lo})_c = f_{i-f} + \left| f_T - f_D \right| \tag{17}$$

$$(f_{lo})_r = f_{i-f} + \left| f_T + f_D \right| \quad . \tag{18}$$

The closing case image frequencies are

$$(f_{image})_c = (f_{lo})_c + \left| f_T - f_D \right| \tag{19}$$

which reduces upon substitution of Eq. (17) into (19) to

$$(f_{image})_c = f_{i-f} + 2 \left| f_T - f_D \right| \quad . \tag{20}$$

Similarly the receding case image frequencies are

$$(f_{image})_r = f_{i-f} + 2 \left| f_T + f_D \right| \quad . \tag{21}$$

The equation for the photomultiplier output, image,and local oscillator frequencies are shown plotted in Figure 8. As required no spurious signals enter the intermediate frequency amplifier. The choice making f_T larger than the maximum doppler frequency $(f_D)_{max}$ is also dictated by the requirement that no ambiguities ever be present at the IF frequencies and that the system operate down to zero doppler frequency. For, as f_D approaches f_T then in progression f_{PM}, f_{lo} and f_{image} are allowed to enter the IF bandwidth.

If a downward frequency translation had been chosen then the receding and closing cases would be interchanged, the magnitude of f_T would be larger than $(f_D)_{max}$ although $f_L - f_T$ would be less than $f_L - f_D$.

A numerical example applicable to the system described is informative. The photodetector for this system is the RCA type C70045C. This tube is a central electrode type photomultiplier with a S-20 surface and a signal rise time of 0.5 nanosecond. The measured 3 frequency response of the tube is 0 to 1 Gc/s. The laser local oscillator would be the single frequency Spectra Physics Model 119. When the laser is stabilized to its gain curve it has a long-term stability of better than 1 part in 10^8. It has a tunable range of about 1 Gc/s. If the local oscillator were offset from the transmitter laser by 500 Mc/s and the IF amplifier is 10 Mc/s wide at 30 Mc/s, then the doppler coverage in one direction would be 460 Mc/s and 500 Mc/s in the other direction.

The doppler frequency coverage of a single translation is determined by the amount of frequency translation. If equal coverage is desired for both receding and closing targets then a translation as described in Figure 8 is applicable. The doppler frequency coverage for either receding or closing cases could be doubled if only one type of coverage were necessary. Also if both upward and downward frequency translation were used depending upon whether the target is closing or receding, the double coverage could be instrumented by appropriate switching of the frequency translation direction.

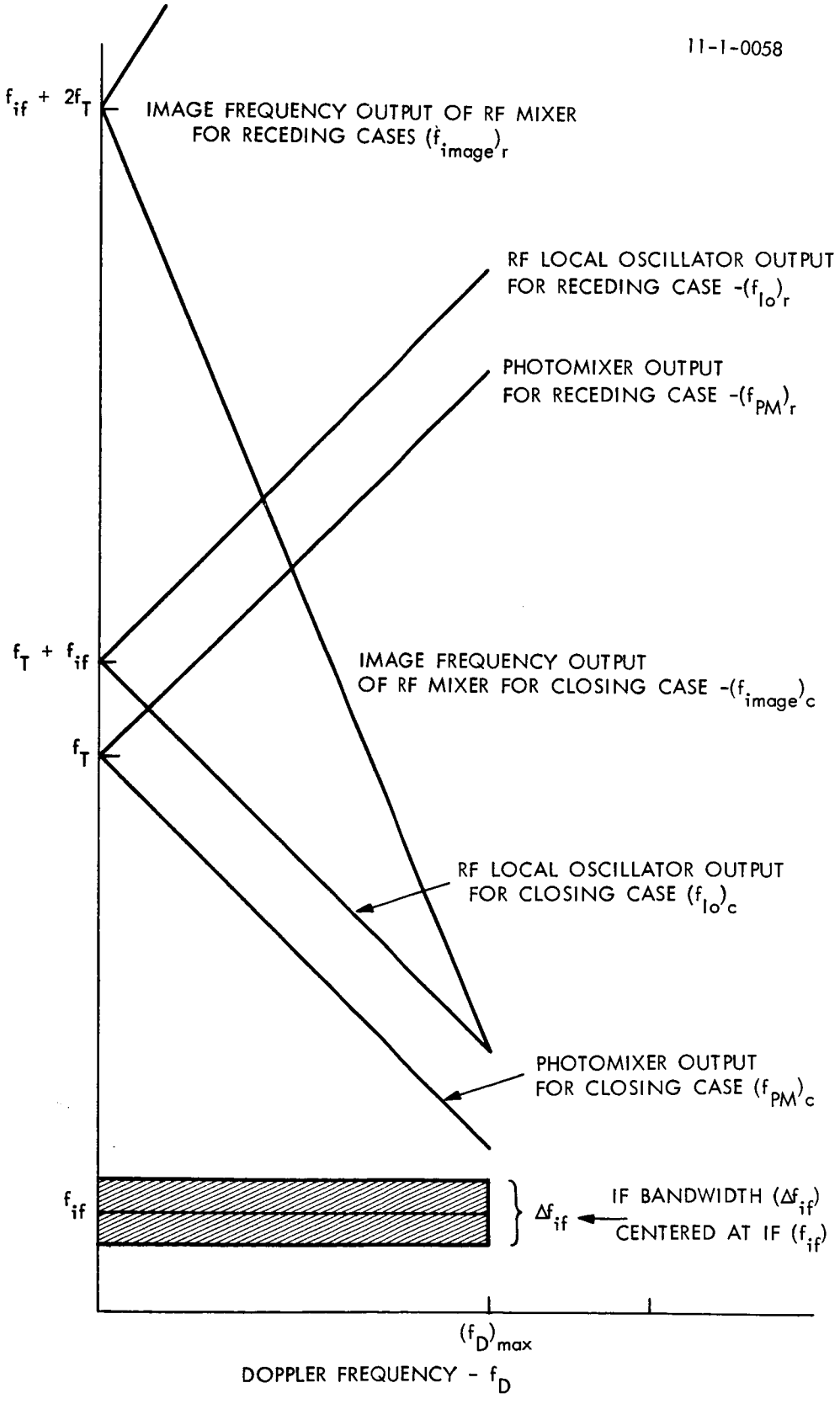

Figure 8. RF Mixer Output Versus Doppler Shift Frequency.

Obviously there are many combinations of coverage that could be utilized. The only restrictions on any of the many alternatives are the upper limit of photomultiplier response and the necessity to keep the image, photomultiplier, and local oscillator signals out of the IF bandwidth. If low doppler and thus low frequency coverage were eliminated, there would be no need for any frequency translation when the doppler signal lies within the photomultiplier bandwidth. Schemes where the IF amplifier frequency lies in the middle of the doppler range could be instrumented if elaborate switching were used to change the IF as undesired components, approached the intermediate frequency bandpass.

If the optical beat frequency increases beyond the photomixer response then a fixed translation can be used to bring the new doppler spectrum range in to the bandwidth of the photomultiplier. This is illustrated in Figure 9. Control of the bandswitching would be determined in part by measuring the value and slope of f_{lo}. This is easily done since the local oscillator is voltage tunable.

2.2.2 Considerations for Design of Frequency Tracking Loop

2.2.2.1 Typical Loop Description

The frequency tracking loop provides the automatic tuning to keep the difference frequency constant at the intermediate frequency as the doppler frequency changes. Eventually the tracking loop should provide search and acquisition capabilities since momentary or prolonged disruption of the optical link could occur.

The tracking mode of operation of a possible AFC is shown in Figure 10. The laser signal containing the doppler shift is mixed with the optical local oscillator signal in the photomixer. The output of the detector contains the doppler frequency. As discussed previously the optical local oscillator is offset from the transmitter laser frequency. To increase the doppler coverage other translators are shown. The output of the photomultiplier is a signal of variable frequency (for an accelerating target) contained between the limits of operation of the detector. The signal is mixed in the RF mixer with the output of a voltage-controlled oscillator.

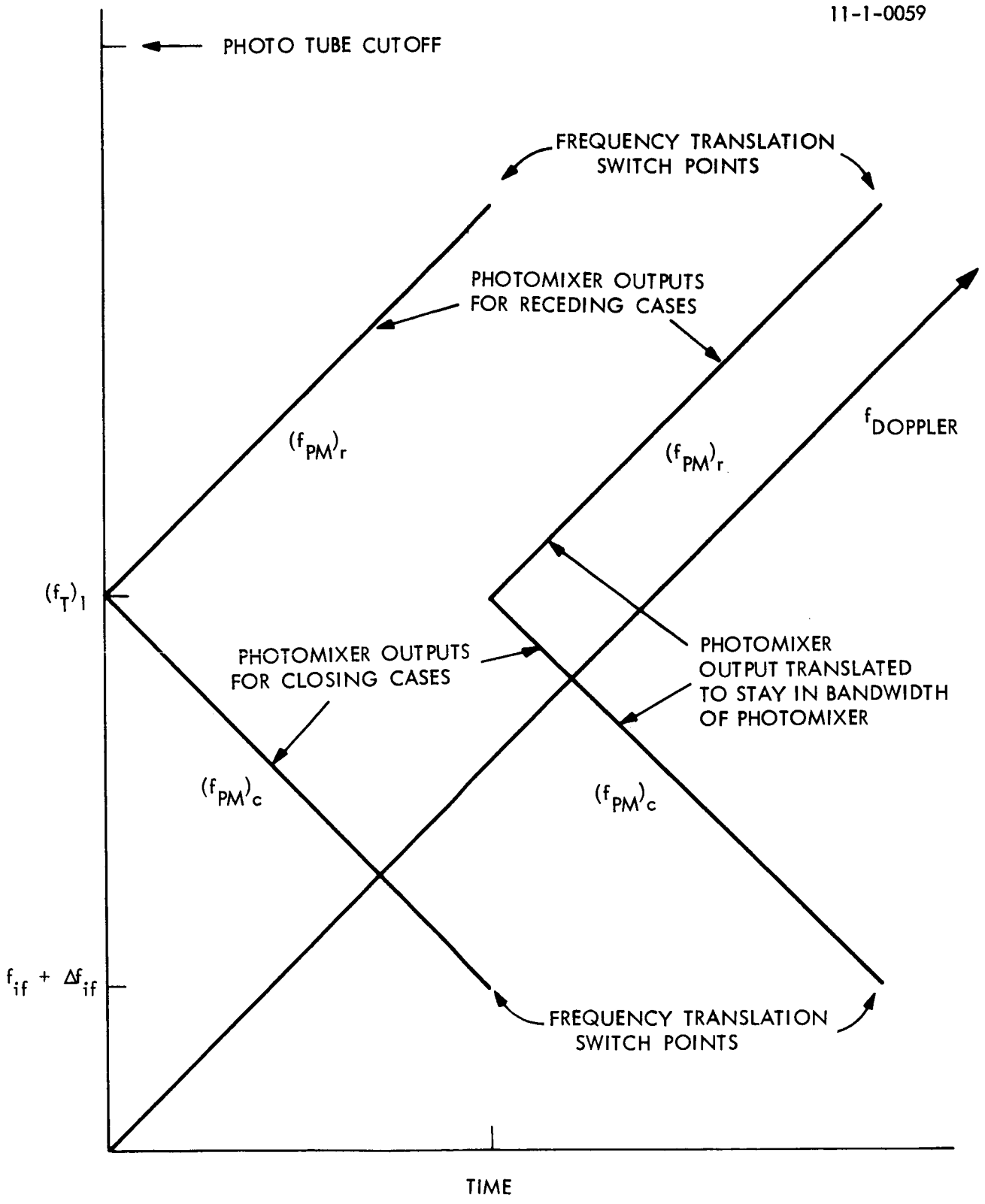

Figure 9. Translated Doppler Frequency Curve.

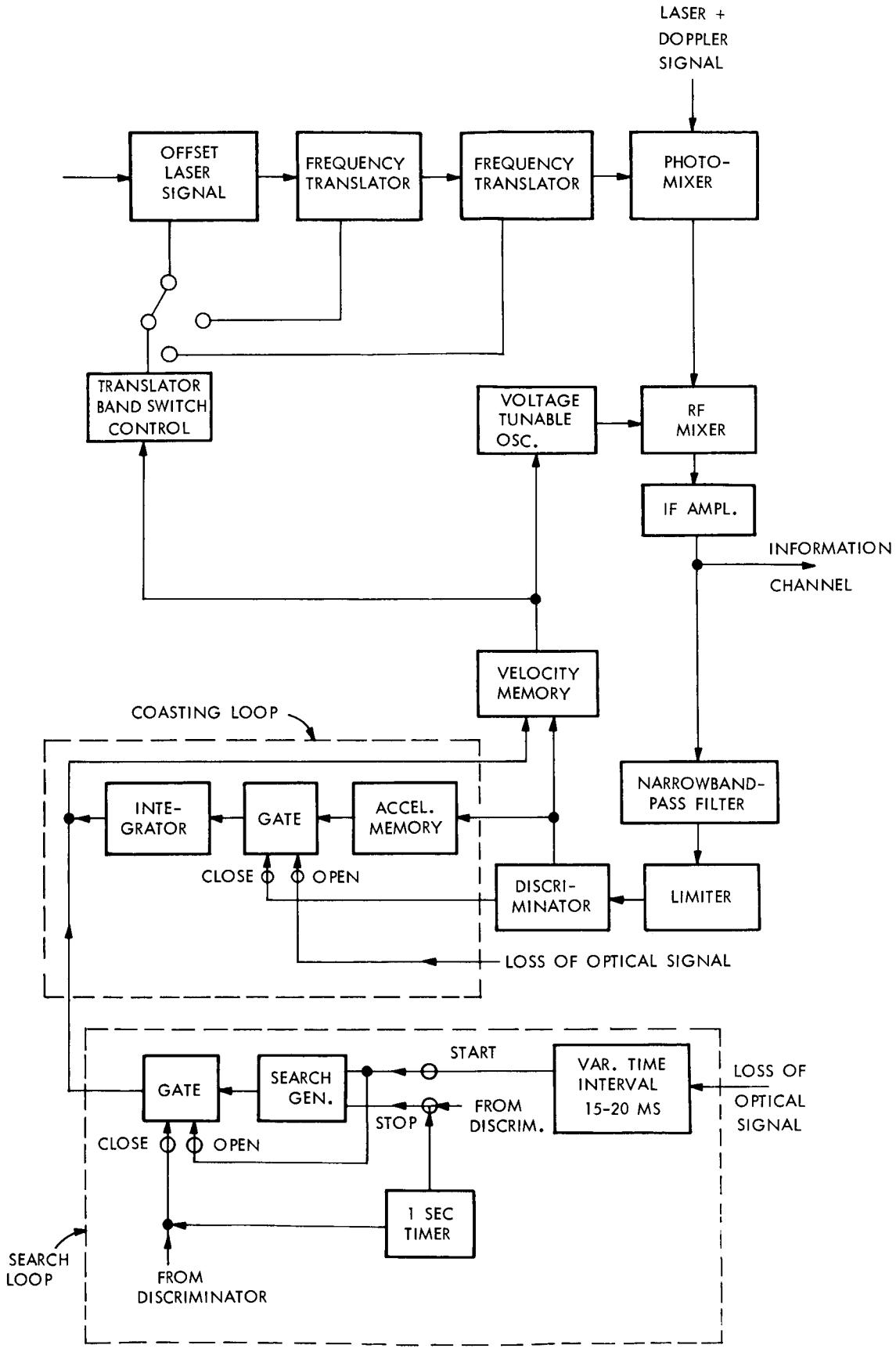

Figure 10. AFC Loop Block Diagram.

Due to the closed-loop operation an error signal is developed at the discriminator which keeps the difference frequency between the two signals at a constant IF value. The bandwidth of the AFC loop is chosen at the minimum value consistent with the expected rates of change of frequency. This insures a relatively high signal-to-noise ratio. For this reason, a narrow bandpass filter is used. The discriminator output is integrated to provide velocity memory and also a suitable command voltage for the sweep oscillator.

As the sweep oscillator reaches a preset frequency, provision is made to switch the frequency translator. This function is achieved by the bandswitch control.

In case of loss of optical return, the coasting mode takes over. In essence, it consists of a linear extrapolation of the frequency versus time curve over a limited time interval as determined by the available AFC loop bandwidth and the actual parameters of the target. The operation of the loop is as follows: the loss of optical signal opens a gate to integrate the signal stored in the acceleration memory, this is added to the velocity information, thus providing a linear continuation for the command voltage of the sweep oscillator. In case of return of optical signal during the coasting period, the discriminator output closes the gate and normal tracking operation is resumed. An analysis of the maximum coasting time is presented in Appendix A.

If, however, no locking is achieved during the preset coasting time, the search function sets in. In the search mode, the coasting is continued but superimposed on it is a growing amplitude constant slope search pattern. The amplitude of the search pattern is determined such as to cope with eventual acceleration variations of the target during the searching period. The search generator is initiated by a signal marking the end of the coasting period, given by the variable time interval generator. This also opens the gate for the search signal and triggers a one-second timer. When the signal is reacquired, the discriminator closes the gate for the search signal. However, if the signal is not reacquired during the one-second time interval, the search is interrupted because the acquisition capabilities of the search loop are exceeded. An analysis of the search function is given in Appendix A.

2.2.2.2 Frequency Translator Bandswitching

The optical local oscillator frequency is translated when the doppler frequency reaches a value near either extreme of the range of coverage for a given translation. The lowest range given in Section 2.2.1 was illustrated in Figure 10. In this example for receding targets with increasing doppler frequencies the switching point is determined by the photomixer cutoff frequency. For closing targets with increasing doppler frequencies the limit was determined by the choice of the IF bandwidth and frequency. It was also noted that the frequencies could be determined by measurement of the voltage controlling the RF local oscillator. Figure 9 shows the output of the photomixer as a result of a second frequency translation demanded by increasing doppler frequency for both closing and receding targets. In this figure the receding target coverage was not allowed to extend to the upper limit of the photomultiplier in order to permit the receding and closing target frequency translations to be the same. The upper limit of the intermediate frequency restriction and the corresponding gap between the upper limit for receding targets has been exaggerated in the figure. Actually, $f_{if} + \Delta f_{if}$ may be about 40 Mc/s, and the value of f_T would be about 500 Mc/s. Thus, only about 10 percent of the bandwidth of a photomultiplier responding from 0-1 Gc/s is not used. In Figure 9 the doppler frequency is shown increasing linearly with time. In reality there can be fluctuations occurring at bandswitching points. Overlapping of band coverage can eliminate this difficulty.

2.2.2.3 Loop Bandwidth

The AFC loop bandwidth is determined by the maximum rate-of-change of the input frequency expected. For instance, the maximum frequency deviation rate due to the drift of a single frequency laser such as the Spectra Physics Model 119 has been estimated by Spectra Physics to be 10^8 c/s^2. If the error was required to be half of the AFC loop bandwidth of $\Delta f_{c/2}$ than the necessary loop bandwidth (gain-crossover frequency) would be

$$\frac{\dot{f}}{\Delta f_c} = \frac{\Delta f_c}{2} \tag{22}$$

which for

$$\dot{f} = 10^8 \text{ c/s}^2$$

$$\Delta f_c = 5.7 \times 10^3 \text{ c/s} .$$

In a similar fashion the bandwidth necessary to accommodate the rate of change of the received signal frequency due to relative motion between the system end points can be calculated. For a mission such as a missile being launched straight up from a launch pad at a certain distance from the tracker, the maximum rate-of-change of doppler occurs at an elevation of $\pi/4$ radians and is proportional to the $\sqrt{2}$ times the missile acceleration. For a missile undergoing an acceleration of 100 ft/s^2 the maximum doppler rate of change is approximately 150 Mc/s^2. To track this rate of change in frequency on the incoming signal the bandwidth must be 6.7 kc.

The accuracy with which the AFC loop can operate will be a function of the signal-to-noise ratio at the discriminator input. The tracking error δf in the loop bandwidth Δf_c is approximately

$$\delta f = \frac{\Delta f_c}{N} \tag{23}$$

where N is the signal-to-noise voltage ratio. In the range calculation a minimum value of N has been required to be 10 in a 4 Mc bandwidth. If Δf_c is 6 kc as calculated above, the maximum tracking error will be approximately $\delta f = 23$ c/s.

2.2.2.4 IF Amplifier and Automatic Gain Control

The IF amplifier must have a bandwidth adequate to pass the video information, and the AGC circuits associated with it must have dynamic range and speed of response adequate to compensate for the changing signal amplitude as the distance between the operating sites varies and the intervening atmosphere causes fades. The time constants of the AGC are determined with the signal fading rate produced by atmospheric turbulence. The performance of the present optical superheterodyne receiver over the long atmospheric paths as described in Section 2.1 has led to an initial estimate of the fading and fading rate. These observations indicate that

the maximum average fading dynamic range is about 10:1 for a day with severe atmospheric turbulence. Our estimate of the maximum rate lies in a range between 100 and 500 c/s. These values along with signal-range calculations for the experiments give the preliminary design specifications for the IF amplifier and the AGC.

2.2.3 Detectors

2.2.3.1 Photoemissive Detectors

In an optical superheterodyne receiver using a photoemissive detector the detection of the beat frequency is performed at the photosurface. At low light intensities the resultant currents are small even when large local oscillator power is used. Maximum receiver sensitivity is obtained when the signal-to-noise ratio P_{so}/P_{no} as given by Eq. 1 of Reference 2

$$\frac{P_{so}}{P_{no}} = \frac{QP_s}{h\nu\Delta f} \tag{24}$$

where

Q is the quantum efficiency

P_s is the signal power

$h\nu$ is the energy per photon

Δf is the electrical bandwidth.

The sensitivity expressed by Eq. (24) will be degraded if the amplification following the photosurface detection process introduces a noise power greater than $h\nu\Delta f/Q$. In photomultipliers the secondary emission amplification introduces some noise. This additional noise degrades the value of Eq. (24) about one dB in well-designed and operated tubes.[4] In photomultipliers this "noiseless" amplification is sufficiently large to eliminate further signal-to-noise degradation by the amplifiers following the tube output. Present day photomultipliers are limited in frequency response to at most 1 Gc/s. Standard fast rise time tubes have 3 dB cutoff frequencies of about a hundred megacycles. Developmental models of faster

photomultipliers have been designed and constructed.[5] The objective of the developmental model RCA type C70045A is to produce a photomultiplier whose output pulse rise time is less than 0.5 nanosecond. This rise time corresponds to a 3 dB cutoff of 700 megacycles. Traveling wave phototubes (TWP) respond to higher frequencies. These tubes are also in the developmental process.

Attempts to include multiplier stages in traveling wave phototubes are being pursued by RCA under contract with the Signal Corps. Transmission secondary electron multiplication is used in these tubes. A fundamental difficulty with these multipliers is caused by burnout due to excessive photo current. A major advantage of the optical superheterodyne technique is its ability to discriminate against noncoherent light background. To perform this discrimination the local oscillator power must be made large compared to background levels. Local oscillator powers of at least 0.1 to 1 microwatt will be required for good background discrimination. For example see Reference 6, page 24. Present TSEMs seem to be limited to current densities of about 1 to 10 $\mu a/cm^2$.[7] Using a S-20 surface and a local oscillator power of 1 microwatt of 6328 Å laser light the resultant current is 2.5×10^{-2} μa. Considering that it is desirable to make the mixing area as small as possible to reduce the beat cancellation effects of signal and local oscillator misalignment, care must be used in the application of these tubes to an optical superheterodyne receiver. The design criterion for these tubes when applied to the optical superheterodyne receiver must include consideration for the large local oscillator powers that are required for background discrimination capabilities.

If the local oscillator power can be made large enough then no TSEMs would be required because of the heterodyne amplification process. An added feature to the elimination of TSEMs would be the increased frequency response of the phototube. At the present time TSEMs have been shown to work out to 1.1 Gc/s.[7]

The criteria to determine the amount of local oscillator power required should be that the amplifiers following the phototube should not degrade the phototube noise figure. Ideally the noise figure of a phototube should be equal to 1/Q where Q is the quantum efficiency of the surface.

Actually the noise figure is given by the expression

$$F_{opt} = \frac{1}{Q}\left[1 + \frac{FkTh\nu}{2RG^2Qe^2P_r}\right] \qquad (25)$$

derived in Appendix D.

The first term in the brackets is unity and refers to the noise figure of the photosurface itself. Thus the noise figure of a photosurface is the reciprocal of the quantum efficiency. The second term includes the effects of the noise figure of the amplifier following the phototube output. This expression was used in Eq. (76) of Reference 2 to define the required load resistance value for phototube operation. Normally the term RG^2P_r in the denominator should be made large to make the receiver operation limited only by the photosurface. When G^2 and R are fixed by other design considerations then only P_r can be controlled independently to set the system noise figure.

Photomultipliers

Photomultipliers usually have G values greater than 10^6, thus even when used with 50 to 100 ohm loads for wideband operation the noise of the following amplifier is small. For example, consider the type 7265 photomultiplier. Conservative parameters that can be substituted in Eq. (25) are:

$F = 4$

$T = 300^{o}k$

$k = 1.38 \times 10^{-23}$ joule/deg

$h\nu = 3.1 \times 10^{-19}$ joule for 6328 Å wavelength

$R = 50$ ohms

$G = 10^6$

$Q = 0.05$ at 6328 Å

$e = 1.6 \times 10^{-19}$ coulomb .

Substituting these values gives

$$F_{opt} = 20\left[1 + \frac{2.5 \times 10^{-12}}{P_r}\right] . \qquad (26)$$

Thus for local oscillator powers sufficient to discriminate against background noise

$$F_{opt} = 20$$

which is the noise figure for the photoelectric surface. To improve on this figure better surfaces would have to be found. Consequently photomultipliers neglecting the noise introduced by the secondary emission amplification are limited only by the quantum efficiency of their photosurface.

Traveling Wave Phototubes

Traveling wave phototubes have been made to cover different microwave bands. Present models[7,8] are being built mostly in the 1-4 Gc range. Special models[9] have been built to cover frequencies from 10 to 20 Gc. In addition image dissector type TWP have also been constructed.[10]

The equivalent output resistance of traveling wave phototubes depends upon the helix length. Data from Report No. 4, Figure 17 of Reference 8 shows the equivalent output resistance for a 2 inch helix tube to be 70 K ohms and for an 8 inch helix to be 300 K ohms. These measurements were made at 3 Gc. Other data from both Sylvania[8] and RCA[7] shows resistance values of nearly 1 M ohm at this frequency.

The output resistance[8] has been shown to be independent of photocurrent at values of signal current less than 10 μA. This is the range in which a superheterodyne receiver would operate. For example the responsivity of an S-20 surface is 2.5×10^{-2} $\mu A/\mu W$ at 6328 Å. The rms beat photocurrent is given by the expression

$$\bar{i}_s = \rho\sqrt{2P_sP_r} . \qquad (27)$$

For $\bar{i}_s$ to be greater than 10 μa the value of the radical would have to be

$$\sqrt{2P_sP_r} > 400\ \mu W.$$

This is a much larger beat signal than would be generally encountered at the signal levels we are considering. Thus, over the operation range of consideration the equivalent output resistance of the traveling wave phototube may be considered a constant for a given helix length.

Typical values may now be considered for evaluating the noise figure of a traveling wave phototube. The previous numerical values (except for G and R) may be substituted in Eq. (26). A conservative estimate for R from Reference 8 Report 4 is 200 K ohms. The value of F for a low noise S band traveling wave phototube amplifier is 4. Retaining Q, G and P_r as parameters, Eq. (26) becomes upon substitution

$$F_{opt} = \frac{1}{Q}\left[1 + \frac{5 \times 10^{-7}}{QG^2P_r}\right] . \qquad (28)$$

The traveling wave phototubes made by Sylvania have no secondary emission amplification, thus G = 1. Figure 11 shows F_{opt} plotted as a function of local oscillator power for S-20 and S-1 surfaces. Photomultipliers have S-20, S-11 and S-1 surfaces are also plotted for reference. The data shows that this S-20 traveling wave phototube will operate optimally when a local oscillator power of 0.1 m watt is used. Figure 12 shows curves for an S-20 traveling wave phototube with one and two stages of multiplication. Each multiplier has a gain of 4. The figure shows that use of TSEMs will relax the local oscillator power requirements.

Unfortunately present developmental S-20 traveling wave phototubes do not have surfaces which achieve the full S-20 efficiency.

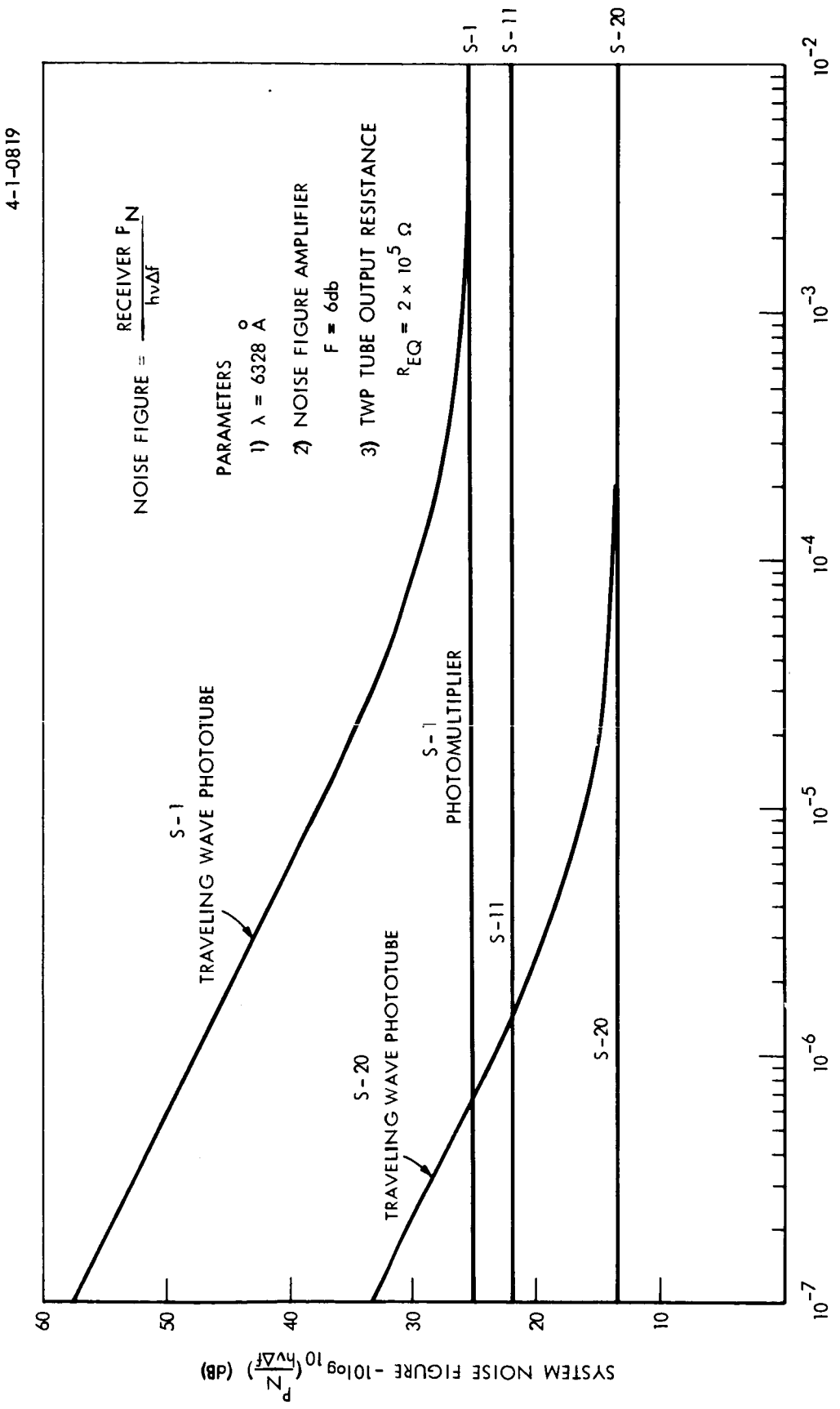

Figure 11. Optical Superheterodyne Receiver Noise Figure.

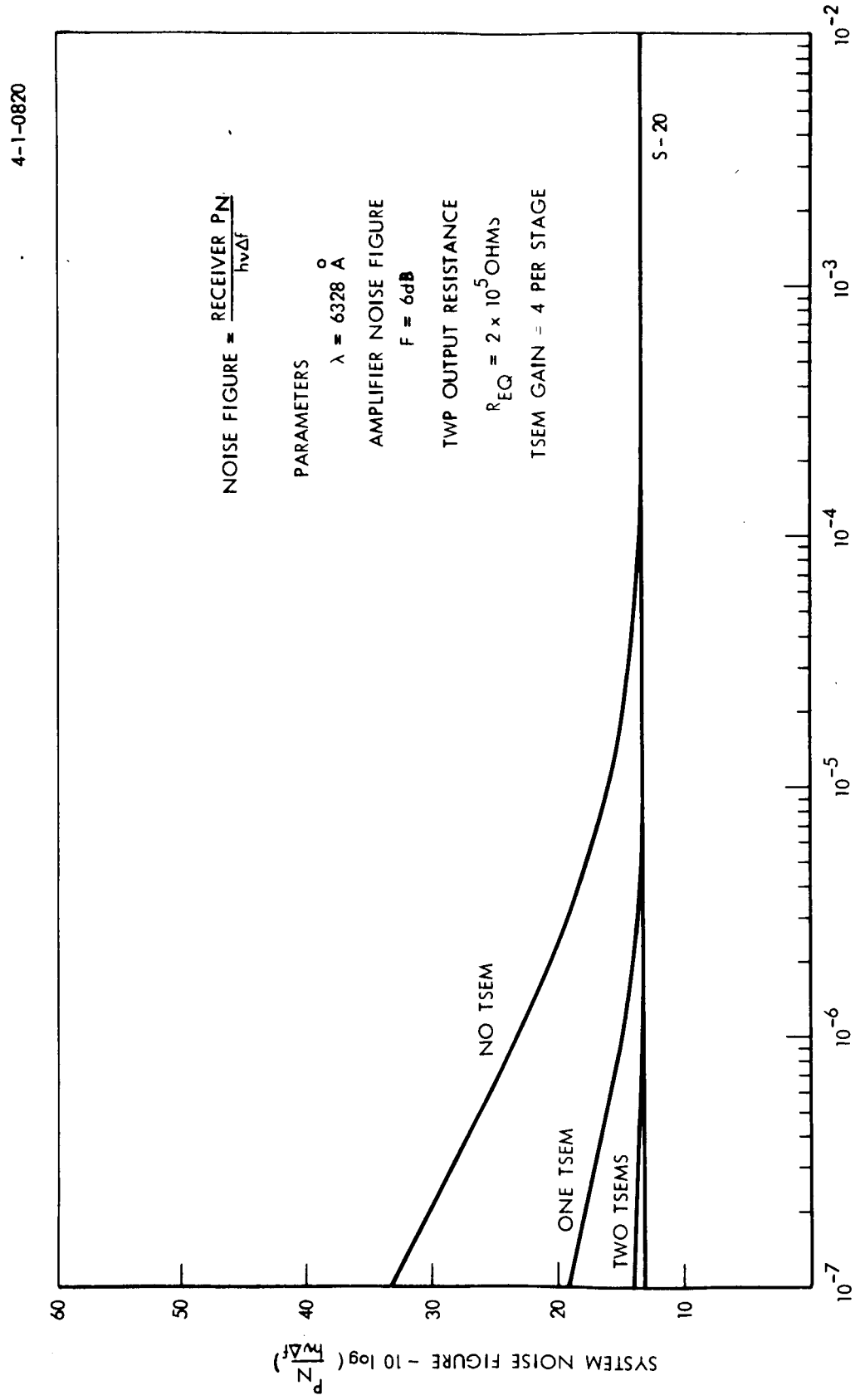

Figure 12. Optical Superheterodyne Noise Figure Using TWP with TSEM Amplification.

2.2.3.2 Solid State Photodiode Detectors

Use of solid state photodiodes[11,12] as photomixers have been considered. These devices as yet appear to lack sufficient internal gain for the application. The equivalent resistances of these diodes range from 1500 ohms at 2 Gc to 50 ohms at 10 Gc, according to Anderson[12]. This is well below the equivalent output resistance of a traveling wave phototube. At present the traveling wave phototube and consequently the solid state photodiode require a greater internal noiseless gain even in the heterodyne application before they become competitive with the fast rise time photomultiplier.

2.2.4 Local Oscillator

2.2.4.1 Laser Source

The laser local oscillator source should be nearly identical with the transmitter source. Multilongitudinal mode lasers either as a transmitted or receiver local oscillator can not be used. These lasers with their multifrequency outputs would make the doppler tracking problem more severe because of the large number of images that would be produced. An analysis showing the spectral content of a coherent laser system utilizing multifrequency lasers, presented in Appendix C, demonstrates this complexity. In addition, with multifrequency, laser a repetitive signal fading condition dependent upon range will produce additional anomalies. This phenomenon has also been studied and the details presented in Appendix B. Consequently the use of a single frequency laser for a local oscillator source is a necessity.

The laser local oscillator noise and power requirements are discussed in the literature[2]. Ideally sufficient monochromatic power should be available to permit discrimination against random noise producing sources such as reflected or scattered sunlight. Also the noise produced at the output of the photomixer due to the local oscillator should not exceed the expected shot noise level for the corresponding local oscillator power. Existing single frequency lasers apparently will be satisfactory. A Spectra Physics Model 119 laser has been evaluated for this purpose.

The monochromatic power output is approximately 100 μW. Anticipated severe background levels such as a bright cloud should not exceed 0.1μW in the system described in Section 2.1. Measurements of the noise in a 4 Mc/s bandwidth for the laser tested showed the noise to be "white." The rms value of the noise exceeded by 3 times the minimum slot noise level expectations for 100 μW of power.

The stability of the local oscillator is important. The specifications on the Model 119 state that the long term stability for a $\pm$ 1^{o}C ambient temperature change is $\pm$ 75 Mc/day. If the laser is stabilized to its gain curve by a servo the stability becomes $\pm$ 5 Mc/day.

Present estimates made in private communications between ourselves and Spectra Physics has resulted in an estimate of the short-term rate of change of frequency of 10^8 c/s^2. The present design of the RF frequency* tracking loop is based on this estimate.

The laser is tunable over a 1200 Mc range-via a voltage controllable input at a rate up to 3 kc. The length of the cavity is the parameter that is varied. Thus this laser can be used to provide a fixed offset from another transmitter laser or could even be used in a frequency tracking loop to cover a doppler range, of 1200 Mc or more depending upon the system format and photomultiplier bandwidth. Use of a tunable laser in the doppler frequency tracking application depends upon the evaluation of the short term stability and the resetability of the laser. Until this has been done, use of the tunable RF system to compensate for laser instabilities and also for doppler frequency tracking is preferred.

2.2.4.2 Frequency Translators

Eventual extended performance of the system by the incorporation of an optical frequency translator can be anticipated. These translators have the potential of shifting the laser frequency by a single sideband suppressed carrier modulation technique. These translators have been constructed and operated at frequencies of 30 kc/s with further engineering effort they could be extended to a frequency coverage of $\pm$ Gc/s. Sylvania's effort in frequency translation techniques has been an out-growth of the development of a wideband phase modulator. This work is described in the literature.[13]

*See last paragraph on page 3.

The frequency translator has been developed under company sponsorship. A forthcoming paper in "Applied Optics" will describe this device. During the past year a company constructed device was tried in the superheterodyne receiver and successfully operated at 30 kc/s. Using the same techniques this device could be extended to about 4 Gc/s.

For a satellite-to-ground application, if we consider that the satellite is traveling with a linear velocity of 24,000 f/s the maximum doppler shift produced would be about 24 Gc/s for a 6328 $\mathring{A}$ laser signal. A coverage of $\pm$ 4 Gc/s would correspond to an angular coverage of about $\pm$ 10^{o} about the perpendicular direction between the tracking station and the satellite.

One limitation in application is the 100 watts of modulation power required for the translator. Although they may not be applicable to a satellite system it should be noted that only the one end of a ground-to-space link need be shifted in frequency to perform doppler tracking of a signal. Thus the translation can be performed completely on the ground where there would be no power or weight limitation. Consequently we would expect to extend our doppler tracking techniques by development and without the necessity of a breakthrough in the technology of detectors or materials.

The frequency translator just described uses two phase modulators in sequence, each driven in such a manner that the sidebands have differing states of polarization so that the desired sideband can be selected and the other sidebands suppressed by means of a polarizer.

These phase modulators use KDP-type materials for the electro-optic element. Because of the preferred orientation of the modulator crystals this frequency translator device can be constructed in the traveling-wave configuration. Thus wide bandwidth operation is possible.

This frequency translator is shown in the sketch of Figure 13 and the photo of Figure 14. To avoid confusion we will use the coordinate system x,y,z throughout the frequency translator. This coordinate system is not associated with the crystal axes. The first phase modulator crystals are oriented so that the optic axis, [001], is parallel to the x direction and the [110] crystal direction is parallel to the y direction. The

11-1-0060

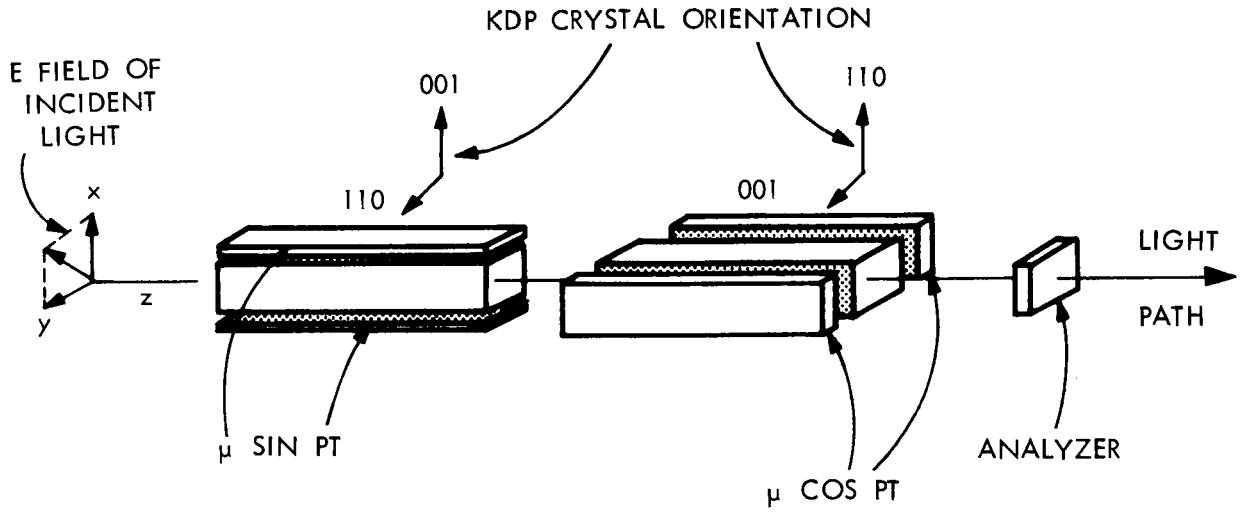

Figure 13. Frequency Translator Using Two Plane Modulators in Tandem.

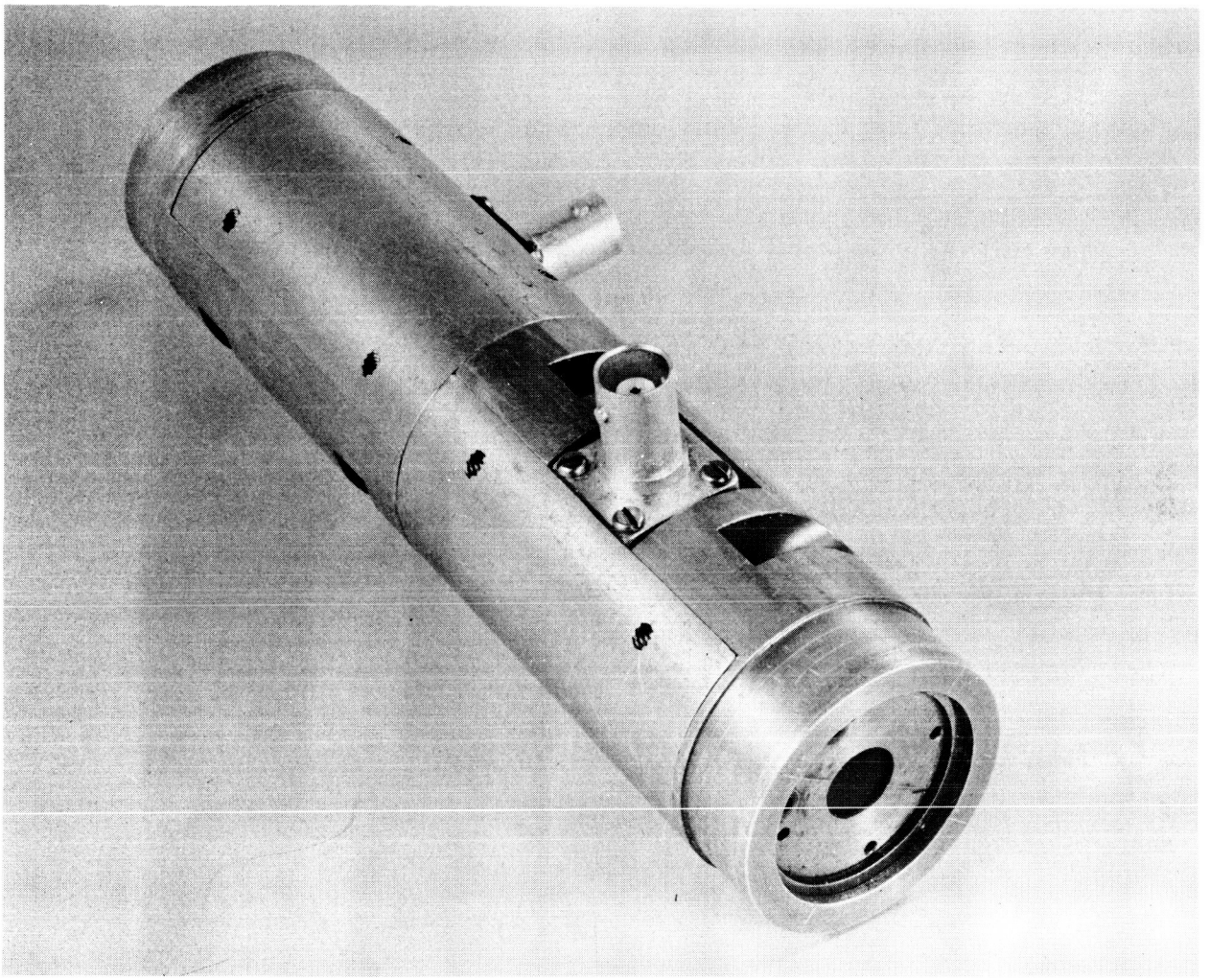

Figure 14. Frequency Translator Photo.

crystals in the second modulator are oriented so that the optic axis is parallel to the y axis of the device and the [110] direction is parallel to the x axis of the device. In both modulators, the modulation electric field is applied parallel to the [001] axis. A phase difference of 90^{o} is maintained between the modulation voltages applied to the two modulators. Thus the first modulator receives a modulation voltage sin Pt and the second modulator receives a modulation voltage cos Pt.

The light travels parallel to the z coordinate with its electric field oriented at 45^{o} to the x axis. The electric field of the light can be considered to be composed of two components, one component parallel to the x axis and the other component parallel to the y. The first modulator imparts a phase modulation to the x component. However, because of the physical characteristics of KDP-type crystals this first modulator does not impart a significant amount of modulation to the y component of the incident light because it is parallel to the optic axis of the KDP crystal. The second modulator imparts a phase modulation to the y component of the incident light. However, the x component which was modulated by the first modulator receives no modulation from the second modulator because it is parallel to the optic axis of the crystal. The effect of modulating these two components is to produce an array of sidebands about the carrier frequency. Like frequency sidebands combine in the output vectorially. Because of the phase difference between the modulation applied to the two modulators there is a unique phase relationship between the two components which make up any one sideband. Hence, each sideband has a unique polarization. One particular sideband can be selected from this array of sidebands by passing the output light through an appropriate polarizing element.

The output of this frequency translator contains the following frequency components:

ω	$\omega + 2p$
$\omega + p$	$\omega - 2p$
$\omega - p$	....

Except for one important case, it is possible to tolerate significant power in these spurious frequency components. The general effect of spurious

frequency components in the laser local oscillator signal is to increase the photo current in the photodetector. This effect is described in detail by Biernson and Lucy.[2] The signal-to-noise ratio of an optical heterodyne receiver is described by Eq. (53) of that paper. The signal power at the output of the photocell is defined as P_s. The predominate noise term in the photocell output current is defined as P_n. The various contributions to this noise term are defined in Table 3 of Biernson and Lucy. Under a reasonable condition of operation the major constituent of these noise terms should be item 4 in this table, the "local oscillator shot noise due to sidebands" in the local oscillator signal. Under these conditions the signal-to-noise at the output of the photocell can be written as

$$\frac{P_{si}}{P_{ni}} = \frac{2\rho^2 P_s P_r}{2e(P_n + P_r)\Delta f} \tag{29}$$

where we have simplified Eq. (53) somewhat. It can be seen from this equation that if P_n is equal to the local oscillator signal power P_r, the signal-to-noise ratio is degraded only by 3 dB from the value it would have under ideal conditions where P_n is equal to 0.

This means that from a signal-to-noise ratio standpoint, at least, a frequency translator which has substantial output at spurious frequencies can be used.

For certain values of the received frequency and the local oscillator laser frequency, intermodulation products between the various frequency components in the output of the frequency translator can fall directly within the IF passband. Since the local oscillator signal is ordinarily between 10 and 100 times larger than the received signal, these spurious signals can be quite large in amplitude. This situation is most likely to occur when the frequency of the received signal is exactly equal to the frequency of the local oscillator laser. Under these conditions, the drive frequency for the frequency translator is just equal to the IF frequency. In order that the "carrier leakage" of this drive frequency be sufficiently low to be undetectable in the IF amplifier it is necessary

for this frequency component to be at least 40 dB below the local oscillator signal.

Our first application for this frequency translator was in a propagation experiment in which one laser was used as the source for both the local oscillator and the transmitted signal. Here these beat products are most troublesome and we found it most convenient to place the frequency translator in the transmitted beam. It was easier to accept the light attenuation in the frequency translator than to implement an automatic null control and perhaps balanced mixer necessary to obtain the desired suppression. We found that the spurious signal could be suppressed to about 2 percent of the desired signal quite easily.

2.3 SPATIAL TRACKING

The spatial tracking function of the optical superheterodyne receiver is of vital importance to the receiver flexibility. The heterodyne optics and subsequent photomixing operation are extremely sensitive to angular changes of the signal direction. The spatial tracking follows the line of sight direction of transmitted signal or transmitter return signal if a retroreflective system is used and maintains the signal along the optical axis of the system. Tests performed upon the optical superheterodyne receiver have shown that the angular limits of operation are $\pm$ 100 μ radians. Thus the angular tracking accuracy of the spatial tracking system must be less than this value. A servo control system using an image dissector as the error sensing detector has been studied, designed, and constructed. The first model of this system used a servo mount which had only a 1 milliradian accuracy. However, a precision mount which will meet the requirements has been designed and at this writing is under construction.

The error sensing technique employed was that commonly used in star tracking systems[14] employing image dissectors. This technique uses a rosette type scan to generate position error signals.

2.3.1 Image Dissector Circuitry

A breadboard model of the error sensing portion of the spatial tracking function was designed and constructed under this contract. A block diagram of the sweep and signal processing circuitry is shown in Figure 15. A rosette-like scan as shown in Figure E-4 was generated by alternately gating and properly phasing a triangular wave from the azimuth to elevation deflection circuits of the image dissector. The triangular wave was formed by integrating the output of a Schmitt trigger circuit. By feeding the output of the integrator back into the input of the Schmitt trigger the amplitude of the triangular wave was made independent of frequency. The frequency of the triangular wave is controlled by the time constant of the integrator.

The output signal from the phototube is amplified and then fed into either the appropriate azimuth or elevation channel in synchronism with the image dissector scanning. Thus azimuth signals are fed into the azimuth control channel and elevation signals into the elevation control. The output signals as described in Atwill[14] are in the form of pulse pairs. There is one pulse pair for each branch of the rosette scan. Thus a full channel scan is represented by two pulse pairs or four pulses. If the target is in the center of the image dissector, the pulses are of equal width and the separation between a pair of pulses is equal to the time required to scan the other channel. Thus for a single rosette cycle for an on-target signal there are two identical pulse pairs for the azimuth channel and two identical pulse pairs for the elevation channel. The fundamental frequency component is the pulse pair repetition rate and is at twice the rosette scan frequency. When a target is off axis the pulse output of a single channel consists of two nonidentical pulse pairs that repeat at the rosette scanning rate. Thus the fundamental component of these two pulse pairs is at the rosette scanning rate. The output of the azimuth and elevation gates are fed to azimuth and elevation amplifiers. Both these amplifiers are tuned to the rosette scan frequency.

On axis singals occur at double this frequency and thus produce no signal in either channel. The off axis fundamental frequency component of the two nonidentical pulse pairs passes through these corresponding amplifiers to the phase sensitive detectors. The phases are compared to

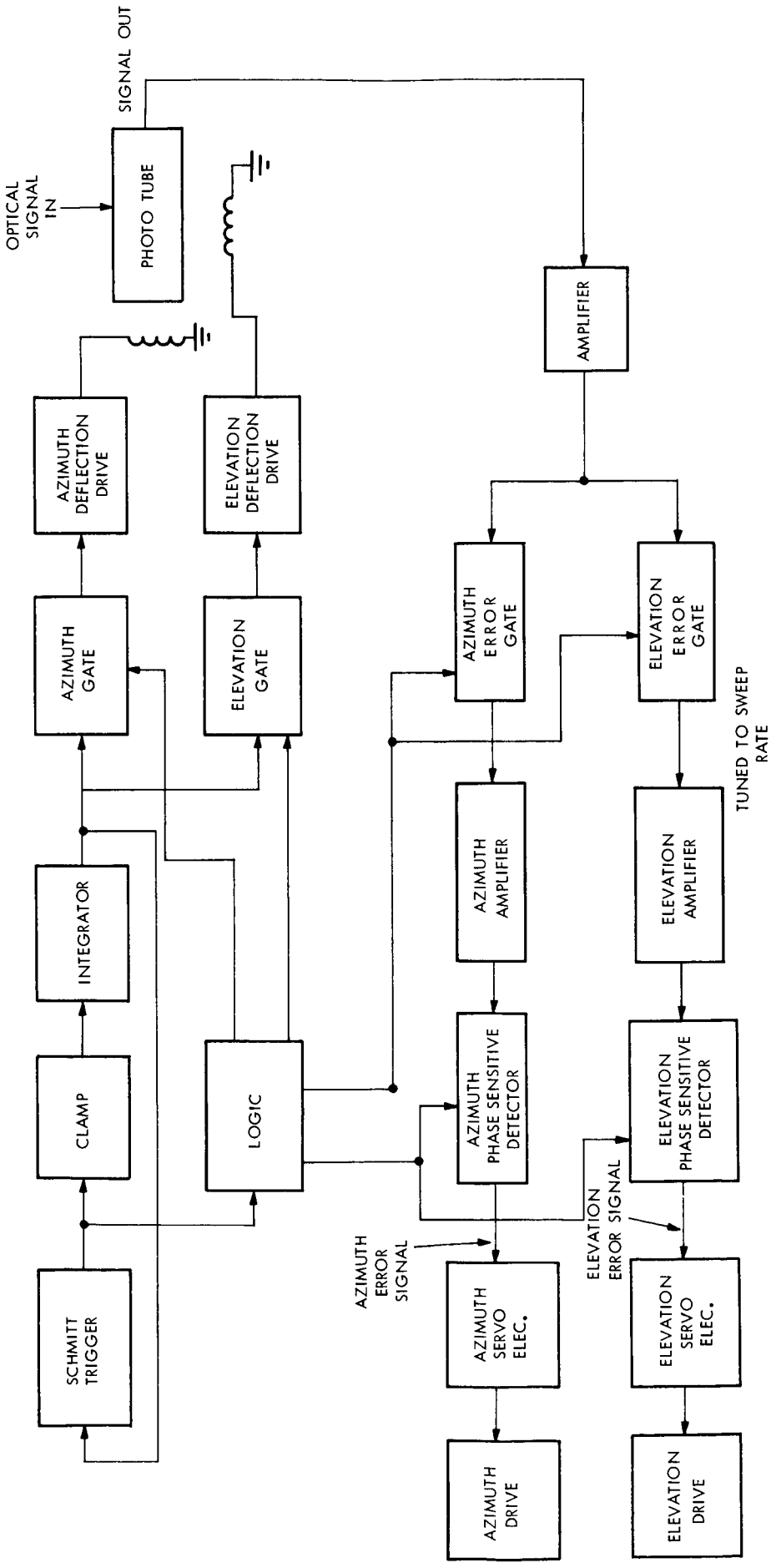

Figure 15. Sweep and Signal Processing Circuitry.

the reference signal generated by the scan generator. The error signal produced is then used to control the servo drive.

The circuitry corresponding to the block diagram has been designed and constructed in breadboard form using all solid state components. Satisfactory operation has been achieved under actual tracking conditions.

2.3.2 Tracking Tests

An evaluation of the image dissector tracking technique in actual daylight tracking tests was made. These tests were performed under our company-sponsored research program. We used a 1 milliradian government surplus radar mount servo-mechanism reconstructed to drive the beam director mirror of the optical superheterodyne receiver. In these tests a retroreflector was mounted on the roof of an automobile. The retroreflector was then illuminated by approximately a 1.5 milliradian laser beam originating in the optical tracking-superheterodyne receiver system and reflected to the target via the beam director mirror. The retroreflector return was again reflected off the beam director mirror to the 8 inch diameter parabolic mirror of the receiver. The signal, focused to a point in the focal plane of the parabola, was then refocused via an auxiliary optical system on to the sensitive surface of the image dissector photomultiplier. The noncoherent photosignal in the image dissector is then scanned over the dissecting aperture of the tube to produce a position error signal for control of the beam director mirror. The automobile was operated along the highway located approximately 1000 feet from the location of the receiver. During the tests the car would start from rest and accelerate to fixed speeds over a course approximately 1500 feet long. The automobile started in a direction which was approximately at right angles to the direction of propagation. Successful tracking to an accuracy of about 1 milliradian was achieved at angular velocities of 4^{o}/second. The tracking accuracy and rate was limited by the government surplus servo mount. The range was limited by the available automobile route. Motion pictures were taken of the tracking experiment.

These experiments have shown us that the error sensing method chosen for spatial tracking in the optical superheterodyne receiver should be applicable to control the precision mount now under construction.

2.3.3 Angle Tracking Servo

The spatial servo control requirements are dictated for the coherent laser system primarily by the necessity of maintaining the optical alignment between the return signal and the local oscillator reference signal which is necessary for efficient heterodyning action. For the spatial tracking function this angular alignment requirement was experimentally determined to be 0.10 milliradian. The new angle tracking servo has been designed so that the total error is less than this value. The total error is the sum of the dynamic error arising from the relative motion between the receiver and the transmitter plus the static error produced by frictional torques and tachometer noise.

The design of the control loop is discussed in detail in Appendix E. This servo will give the desired tracking accuracy in a mission configuration wherein the target accelerates vertically at 100 ft/s^2 from a start position which is 5000 ft from the tracking unit. This control configuration utilizes an image dissector for noncoherent spacial error detection and dc torque motors as prime movers.

The tracking errors in this configuration are shown in Table II.

Clearly all of these errors would not occur at the same time. For example, the maximum angular acceleration does not take place when the controlled member is moving at the maximum angular rate in the projected mission. Also stiction torques do not occur when the output member is moving at the maximum angular rate. It is appropriate to evaluate the rms value of the error caused by maximum angular velocity and tachometer noise error occurring simultaneously which is 0.05 milliradian. The stiction torque and maximum angular acceleration occur together and their rms error equals 0.073 milliradian. Hence we conclude that the total error including both static and dynamic errors will be less than 0.1 milliradian.

The servo design is described in detail in Appendix E. The components are readily available. Motors and tachometers are off-the-shelf

TABLE II

Error	Cause	Pertinent Parameters
0.038 [millirad]	Max. relative angular vel. 0.11 rad/s	Position Loop gain-crossover freq., 30 [rad/s] Integ. Net break freq. ratio, 100
0.067 [millirad]	Max. relative angular accel. 0.02 [rad/s^2]	Position Loop gain-crossover freq., 30 [rad/s] Integ. Net upper break freq. 10 [rad/s]
0.033 [millirad]	Tach. Noise (Inland T-5703) 1% of max. vel. angular vel.	Position Loop gain-crossover freq., 30 [rad/s]
0.03 [millirad]	Stiction load torques 26 [oz-in]	Load inertia, 1.0 [ft-lb.-s^2] Position Loop gain-crossover freq., 30 [rad/s] rate loop gain-crossover freq., 150 [rad/s]

Inland Motors Types, the 100 c/s assumed load resonance can be obtained with the mirror mounted in a properly designed mount, the amplifiers and integral networks require reasonable gains and frequency responses and the image dissector provides the required angular error resolution. It should be noted that the design of this control system is based strictly on a worst-case approach and no attempt has been made to optimize the performance by using time varying gains and a priori knowledge because the system philosophy is to develop the best possible basic controls and to introduce sophisticated techniques as they become necessary to expand the laser tracking system capability.

REFERENCES

1. K. T. Lang, Applied Research Laboratory, Sylvania Electronic Systems, An Experimental Optical Superheterodyne Using Mirror Optics, Research Note No. 451, Waltham, Mass., 11 Feb. 1964

2. G. Biernson and R. Lucy, "Requirements of a Coherent Laser Pulse Doppler Radar," Proc. IEEE, Vol. 51, 1 Jan. 1963, pp. 202-213

3. R.C.A., Research Studies of Quantum Detectors and Mixers, Report No. 7, Contract No. DA36-039-SC90846, Jan.-Mar. 1964

4. J. Sharpe, "Photoelectric Cells and Photomultipliers," Elec. Tech., June 1961, pp. 2-16

5. G. A. Morton, et al., "Design of Photomultipliers for the Sub Milli-microsecond Region," IRE Trans. on Nuclear Science, Vol NS5, Dec. 1958, pp. 98-104

6. Applied Research Laboratory, Sylvania Electronic Systems, Proposal for Development of an Optical Superheterodyne Receiver, Waltham, Mass., Nov. 1963

7. R.C.A., Research Studies of Quantum Detectors and Mixers, Report No. 6, Contract No. DA36-039-SC90846, Dec. 1963

8. R. Targ, D. E. Caddes, B. J. McMurtry, " The Traveling Wave Photo Part 1 and Part 2," IEEE Trans. of Prof. Tech Group on Electron Devices, Vol. ED 11, No. 4, April 1964, pp. 156-170

9. D. E. Caddes, "AKU Band Traveling Wave Phototube," Microwave Journal, Vol. 8, No. 3, March 1965 p. 46

10. R. F. Lucy, "An Experimental Photomixer Image Tube," Proc. IEEE, Vol. 51, No. 1, Jan. 1963, pp. 162-165

11. Lucovsky, et al., "Coherent Light Detection in Solid State Photo-diodes," Proc. IEEE, Vol. 51, Jan. 1963, pp. 166-172

12. L. K. Anderson, "Photodiode Detectors," Optical Masers, Polytechnic Press, Apr. 1963, pp. 549-566

13. C. J. Peters, "Gigacycle Bandwidth Coherent Light Traveling-Wave Phase Modulator," Proc. IEEE, Vol. 51, No. 1, Jan. 1963, pp. 147-153

14. W. D. Atwill, "Star Tracker Uses Electronic Scanning," Electronics, McGraw-Hill, 30 Sept. 1960

APPENDIX A

COASTING AND SEARCH CONSIDERATIONS FOR FREQUENCY TRACKING LOOP

1. ESTIMATION OF THE MAXIMUM ALLOWABLE TIME OF COASTING

In the coasting mode the tracking loop follows a frequency versus time curve which is a linear extrapolation of the actual curve based on available memory data. The difference between the extrapolated curve and the true curve is growing with time therefore the coasting mode must stop when this difference exceeds the bandwidth of the loop. This sets a limit on the allowable time of coasting.

To determine this time we note that the problem is that of determining the interval over which a function differs from its linearized approximation by less then a given amount. For this purpose we use the Taylor expansion of the function

$$v(t + \Delta t) = v(t) + \Delta t v'(t) + \frac{(\Delta t)^2}{2!} v''(t) + \ldots .$$

The condition on Δt is:

$$v(t + \Delta t) - v(t) - \Delta t v'(t) < \Delta v_{max}$$

where

Δv_{max} is a given value dictated by the available bandwidth.

But we can also write

$$v(t + \Delta t) = v(t) + \Delta t v'(t) + R_2(t)$$

where $R_2(t)$ is the remainder of the series, in its Lagrangian form it can be written

$$R_2(t) = \frac{(\Delta t)^2}{2!} v''(t + \theta \Delta t) \qquad \text{with } 0 < \theta < 1 .$$

It is necessary therefore to make $R_2(t) < \Delta v_{max}$. To get an estimate on R_2 we take the worst case when v" reaches a maximum. It is then sufficient to have:

$$\frac{(\Delta t)^2}{2} \quad v''(t_{max}) < \Delta v_{max}$$

which yields

$$\Delta t_{max} \leq \sqrt{\frac{2\Delta v_{max}}{v''(t_{max})}} \quad .$$

It is thus necessary to find the maximum rate of change of acceleration $v''(t_{max})$ in order to estimate the time of coasting.

As an example we consider a missile moving vertically at a constant acceleration α. The doppler frequency is due to the velocity component in the direction of the receiving station as shown in Figure A-1.

$$v_D = v \sin \psi = \alpha t \sin \psi \qquad (A.1)$$

$$\tan \psi = \frac{\alpha t^2}{2r}$$

r is the horizontal distance between the missile launch pad and the observation point.

We wish now to evaluate the maximum rate of change of acceleration. For this purpose we differentiate twice the expression (A.1)

$$a_D = v' = \frac{dv}{dt} \sin \psi + v \cos \psi \frac{d\psi}{dt} = \alpha \sin \psi \, (1+2 \cos^2 \psi) \qquad (A.2)$$

$$v'' = \frac{da_D}{dt} = \frac{da_D}{d\psi} \frac{d\psi}{dt} = \frac{3\alpha^2 t}{r} \cos^2 \psi \, . \qquad (A.3)$$

The maximum of $\frac{da_D}{dt}$ occurs at the point at which its derivative vanishes.

11-1-0062

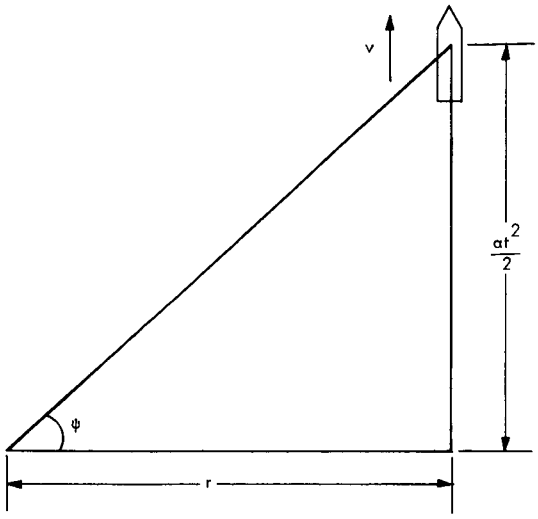

Figure A-1. A Missile Tracking System.

11-1-0063

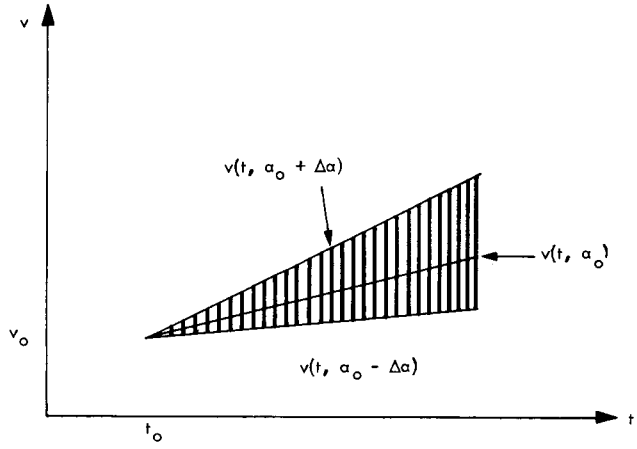

Figure A-2. Search Region for Frequency Loop.

11-1-0064

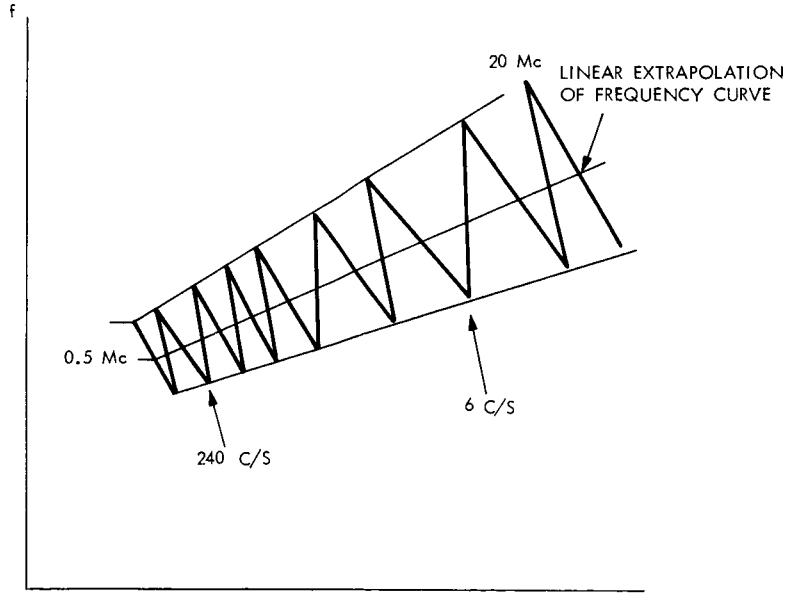

Figure A-3. Frequency Search Pattern.

We must have

$$\frac{d^2 a_D}{dt^2} = \frac{d}{d\psi}\left(\frac{da_D}{dt}\right)\frac{d\psi}{dt}$$

$$= \frac{\cos\psi}{\sqrt{\tan\psi}}\left[-3\sin^2\psi\cos^2\psi - 2\sin^2\psi\sin\psi\cos\psi + \frac{1}{2}\cos^2\psi\right] = 0.$$

By trial we find that

$$\frac{d^2 a_D}{dt^2} = 0 \text{ for } \psi \cong 15^\circ .$$

The corresponding value of rate of change of acceleration can be found from (A.3)

$$v'' = \left(\frac{da_D}{dt}\right)_{max} = 3\sqrt{\frac{2\alpha^3}{r}}\sqrt{\tan\psi}\cos^3\psi\cos^2\psi\Big|_{\psi = 15^\circ}$$

$$v''_{max} = \left(\frac{da_D}{dt}\right)_{max} = 1.2\sqrt{\frac{2\alpha^3}{r}} .$$

Thus the maximum time of coasting is:

$$\Delta t_{max} = \sqrt{\frac{2\Delta_{max}}{1.2\sqrt{\frac{2\alpha^3}{r}}}} = 1.18\left(\Delta v_{max}\right)^{\frac{1}{2}} \alpha^{\left(-\frac{3}{4}\right)} r^{\left(\frac{1}{4}\right)} .$$

As a numerical example let

$$\alpha = 100 \text{ ft/s}^2$$

$$r = 10{,}000 \text{ ft}$$

$$\Delta v_{max} = 5 \times 10^{-3} \text{ ft/s}.$$

This latter figure corresponds to a doppler frequency shift of 5 kc/s for a laser at 6328 Å. Substituting the numbers we obtain

$$\Delta t = 24 \times 10^{-3} \text{ second.}$$

It is also interesting to evaluate the maximum rate of change of velocity from (A.2). The maximum occurs for $\frac{da_D}{dt} = 0$ which yields $\psi = \frac{\pi}{4}$. Thus $\left(a_D\right)_{max} = \sqrt{2\alpha}$. This maximum acceleration places a minimum requirement on the bandwidth of the AFC loop.

2. DETERMINATION OF THE SEARCH PATTERN

The purpose of the search function is to find the signal and to lock on it after the coasting function has failed to do so. It is designed to operate over a wider freqency range and for a longer time than the coasting mode. For this reason the search mode to cope with eventual changes in the acceleration of the target which have occurred form the time the return signal has been lost.

We consider again the problem of tracking the doppler shift from a missile. The velocity of the missile given by

$$v(t,\alpha) = \left[v_o + \alpha\left(t-t_o\right)\right]\sin\psi \qquad \text{for } t > t_o$$

where t_o is the time when the return signal was lost. Let α be the acceleration of the missile for $t > t_o$. We denote by α_o the acceleration prior to t_o, ψ is the elevation angle. We assume that the acceleration of the missile is

$$\alpha = \alpha_o \pm \Delta\alpha \qquad \text{for } t > t_o .$$

Therefore the spread in velocities at any time is given by:

$$\Delta v = v\left(t,\alpha_o \pm \Delta\alpha\right) - v\left(t,\alpha_o\right) = \pm \Delta\alpha\left(t - t_o\right)\sin\psi$$

For the worst case we can take $\sin\psi = 1$. Therefore we will certainly find the velocity in the region bounded by the two curves $v \pm \Delta v$ as shown in Figure A-2. Since we do not know the shape of the curve $v\left(t,\alpha_o\right)$ for $t > t_o$ we extrapolate it linearly from the last known value at $t = t_o$. Such a straight line will differ from the true velocity curve by an amount

$$\left| v\left(t,\alpha_o\right) - v\left(t_o,\alpha_o\right) - a\left(t - t_o\right) \right| < \frac{\left(t - t_o\right)^2}{2}\left(\frac{da}{dt}\right)_{max}$$

so that if we account for that difference we can find the required amplitude for the search pattern.

We recall that the maximum rate of change of acceleration occurs at $\psi = 15^o$ and is given by

$$\left(\frac{da}{dt}\right)_{max} = 1.7\sqrt{\frac{\alpha^3}{r}} \quad .$$

The total amplitude of the pattern overriding the coasting pattern is then

$$A(t) = 1.7\sqrt{\frac{\alpha^3}{r}}\ \frac{(\Delta t)^2}{2} + \Delta\alpha\ \Delta t$$

where

$$\Delta t = t - t_o \quad .$$

Let us consider now a numerical example with

$$\alpha = 100 \text{ ft/s}^2$$

$$r = 10{,}000 \text{ ft}$$

$$\Delta\alpha = 10 \text{ ft/s}^2$$

$$A(\Delta t) = 8.5\ (\Delta t)^2 + 10\ \Delta t \ .$$

If we choose the maximum time of searching as $\Delta t_{max} = 1$ s, at the end of the searching time the maximum amplitude is

$$A(\Delta t_{max}) = 18.5 \text{ Mc/s} \ .$$

Instead of generating the parabolic amplitude patterns given by A(t) it is easier to generate a linear growing pattern which contains A(t) at each instant of time. It can be easily seen that for example the linear pattern given by

$$B(t) = 0.5 + 19.5\ \Delta t$$

satisfies the required condition for $\Delta t < 1$ s. The pattern B(t) has an amplitude of 0.5 Mc/s at $\Delta t = 0$ and of 20 Mc/s at $\Delta t = 1$ s. We now choose a triangular wave as a scanning function. The maximum slope of the triangular wave is dictated by the bandwidth of the AFC loop. For a bandwidth of 5 kc it is found that rates of change of the order of 500 Mc/s can be handled. Such a slope corresponds to a frequency of 240 c/s at an amplitude of 0.5 Mc/s and of 6 c/s at 20 Mc/s. The chosen patternnis illustrated in Figure A-3.

APPENDIX B

AN EXPLANATION FOR THE APPARENT STANDING-WAVE PATTERN OBTAINED IN OPTICAL SUPERHETERODYNE SYSTEMS

1. SUMMARY

It is shown that the standing-wave pattern obtained in an optical transmitter-receiver superheterodyne system is essentially due to the multifrequency character of the laser output. The modulation signal is thus simultaneously conveyed over several carriers at different frequencies. After detection the recovered signal is the vector sum of the partial signals arriving in various amplitudes and phase relationships. This results in an apparent standing-wave pattern, the separation between two successive maxima being given by half of the wavelength corresponding to the minimum difference between the various laser frequencies.

2. THEORY

The optical system on which the standing-wave pattern was observed is given in Figure B-1.

Consider the laser to emit several equally spaced frequencies. The spacing is then given for the dominant TEM_{oo} modes by:

$$f_m = m(c/2b)$$

where

m is an integer in the order of 10^6 for gas masers

c is the velocity of light

b the laser plate separation.

For a 1-m Fabry-Perot, c/2b = 150

form

11-1-0065

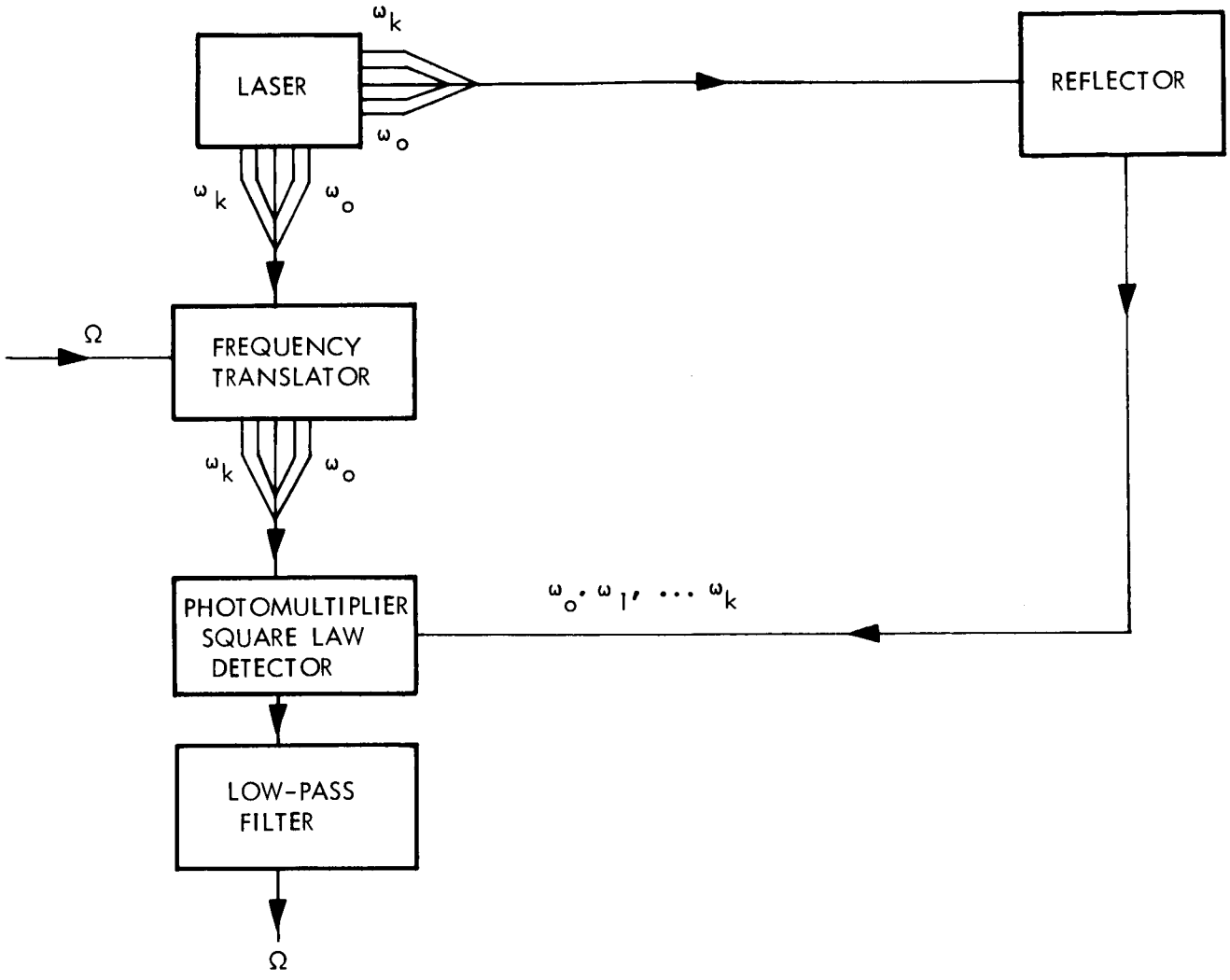

Figure B-1. Block Diagram of an Optical Superheterodyne System.

$$\mathcal{E}(t) = \mathcal{E}_o \cos\left(\omega_o t+\phi_o\right) + \mathcal{E}_1\left(\omega_1 t+\phi_1\right)+ \cdots\cdots \mathcal{E}_k \cos\left(\omega_k t+\phi_k\right)$$

where $\omega_k = \omega_o + k\Delta\omega$ and $\Delta\omega = 2\pi\Delta f$ is a fixed quantity determined by the laser cavity. The received signal is then given by

$$E(t) = E_o\cos\left(\omega_o t+\phi_o \pm \frac{2\pi x}{\lambda_o}\right) + E_1 \cos\left(\omega_1 t+\phi_1 \pm \frac{2\pi x}{\lambda_1}\right)$$

$$+ \cdots\cdots E_k \cos\left(\omega_k t+\phi_k \pm \frac{2\pi x}{\lambda_k}\right) \qquad (B.1)$$

where x is the round-trip path length between the transmitting and the receiving points. The local oscillator signal is of the same form as the transmitted signal except for a fixed frequency translation which we denote by Ω. Thus we have

$$E'(t) = E'_o \cos\left(\omega_o t+\Omega t+\phi_o\right) + E'_1 \cos\left(\omega_1 t+\Omega t+\phi_1\right)$$

$$+ \cdots\cdots E'_k \cos\left(\omega_k t+\Omega t+\phi_k\right) . \qquad (B.2)$$

The two signals given by (B.1) and (B.2) are mixed at the photomultiplier surface. The recovered modulation current is proportional to the square of the total incident signal (square-law detector), we can write

$$I_{mix} \alpha(E+E')^2 = \left[\sum_k E_k \cos\left(\omega_k t+\phi_k \pm \frac{2\pi x}{\lambda_k}\right) + E'_k \cos\left(\omega_k t+\Omega t+\phi_k\right)\right]^2$$

$$= \underbrace{\sum_k E_k^2 \cos^2\left(\omega_k t+\phi_k \pm \frac{2\pi x}{\lambda_k}\right)}_{(a)} + \underbrace{\sum_k E'^2_k \cos^2\left(\omega_k t+\Omega t+\phi_k\right)}_{(b)}$$

$$+ \underbrace{\sum_j \sum_{\substack{k \\ j\neq k}} E'_j E'_k \cos\left(\omega_j t+\Omega t+\phi_j\right) \cos\left(\omega_k t+\Omega t+\phi_k\right)}_{(c)}$$

$$+ \sum_{\substack{j \\ j\neq k}}' \sum_{k}' E_j E_k \cos\left(\omega_j t+\phi_j+ \frac{2\pi x}{\lambda_j}\right)\cos\left(\omega_k t+\phi_k+ \frac{2\pi x}{\lambda_k}\right) \qquad \text{(d)}$$

$$+ \sum_{j}' \sum_{k}' E_j E_k' \cos\left(\omega_j t+\phi_j+ \frac{2\pi x}{\lambda_j}\right)\cos\left(\omega_k t+\Omega t+\phi_k\right) \quad . \qquad \text{(e)} \qquad \text{(B.3)}$$

By examining each of the five terms in the above expansion, we conclude that the only terms which contribute to the signal at the frequency Ω, are contained in the sum (e). In particular we must choose those terms for which j=k. Thus the detected current at the frequency Ω is given by

$$I_{det} = C \sum_{k}' E_k E_k' \cos\left(\Omega t + \frac{2\pi x}{\lambda_k}\right) \qquad \text{(B.4)}$$

where C is a proportionality constant. Since E_k' is proportional to E_k this can also be written

$$I_{det} = D \sum_{k}' E_k^2 \cos\left(\Omega t + \frac{2\pi x}{\lambda_k}\right) \quad . \qquad \text{(B.5)}$$

In the form (B.5) the various modulation components are clearly exhibited with their relative amplitudes and phases. We can now obtain the vector sum of the currents in (B.5) and rewrite it as

$$I_{det} = A \cos(\Omega t - \phi) \qquad \text{(B.6)}$$

where

$$A^2 = D^2 \sum_{k}' \left[\left(E_k^2 \cos \frac{2\pi x}{\lambda_k}\right)^2 + \left(E_k^2 \sin \frac{2\pi x}{\lambda_k}\right)^2\right] \qquad \text{(B.7)}$$

$$\tan \phi = \frac{\sum_k E_k^2 \sin \frac{2\pi x}{\lambda_k}}{\sum_k E_k^2 \cos \frac{2\pi x}{\lambda_k}} \quad .$$

The amplitude A is thus a periodic function of x. The period can be recognized if we write (B.7) in the slightly different form

$$A^2(x) = D^2 \left[\sum_k E_k^4 + \sum_{\substack{k \\ k \neq j}} \sum_j E_k^2 E_j^2 \cos 2\pi x \left(\frac{1}{\lambda_k} - \frac{1}{\lambda_j} \right) \right] \quad . \tag{B.8}$$

But

$$\frac{2\pi}{\lambda_k} = \frac{\omega_k}{c}$$

therefore

$$A^2(x) = D^2 \left[\sum_k E_k^4 + \sum_{\substack{k \\ k \neq j}} \sum_j E_k^2 E_j^2 \cos x \frac{\Delta\omega}{c} (k - j) \right] \quad . \tag{B.9}$$

It is clear now that (B.9) is a Fourier expansion for the amplitude function. The period is given by:

$$\bar{x} = \frac{c}{\Delta f} \quad .$$

For the case Δf = 150 Mc, $\bar{x}$ = 2 meters since x was the total path length (round-trip), the distance between two successive maxima is $\frac{\bar{x}}{2}$ = 1 meter. This agrees with experimental results.

Thus the multicarrier transmission results in an apparent standing-wave pattern.

3. SAMPLE CALCULATION

To illustrate the theory we consider a laser which emits in a spectrum as shown in Figure B-2.

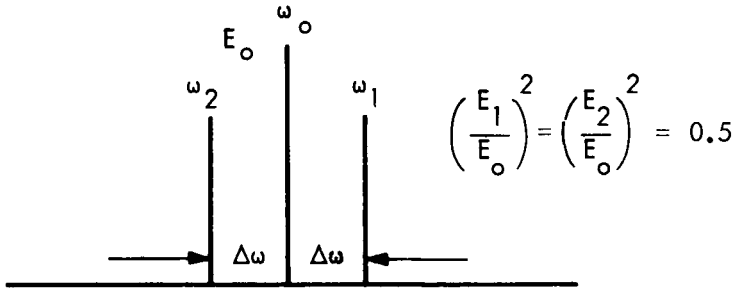

Figure B-2. Laser Spectrum.

From (B.8) we obtain, taking E_0 as unity and dropping the proportionality factor

$$A^2(x) = 1 + E_1^4 + E_2^4 + 2\left(E_1^2 + E_2^2\right)\cos\frac{\Delta\omega x}{c} + 2E_1^2 E_2^2 \cos\frac{2\Delta\omega x}{c} \quad .$$

Substituting the numbers we obtain

$$A^2 = 1.5 + 2\cos\frac{\Delta\omega x}{c} + 0.5\cos\frac{2\Delta\omega x}{c} \quad .$$

In Figure B-3 we have plotted the normalized amplitude versus range variation for the numerical example considered above.

In conclusion standing-wave pattern measurements provide a rapid means for the detection of several frequencies in the output of a laser. Also from the shape of the curve, information can be obtained as to the relative amplitudes of the various frequency components. The smaller the ripple in the amplitude curve the less energy is radiated at the side frequencies.

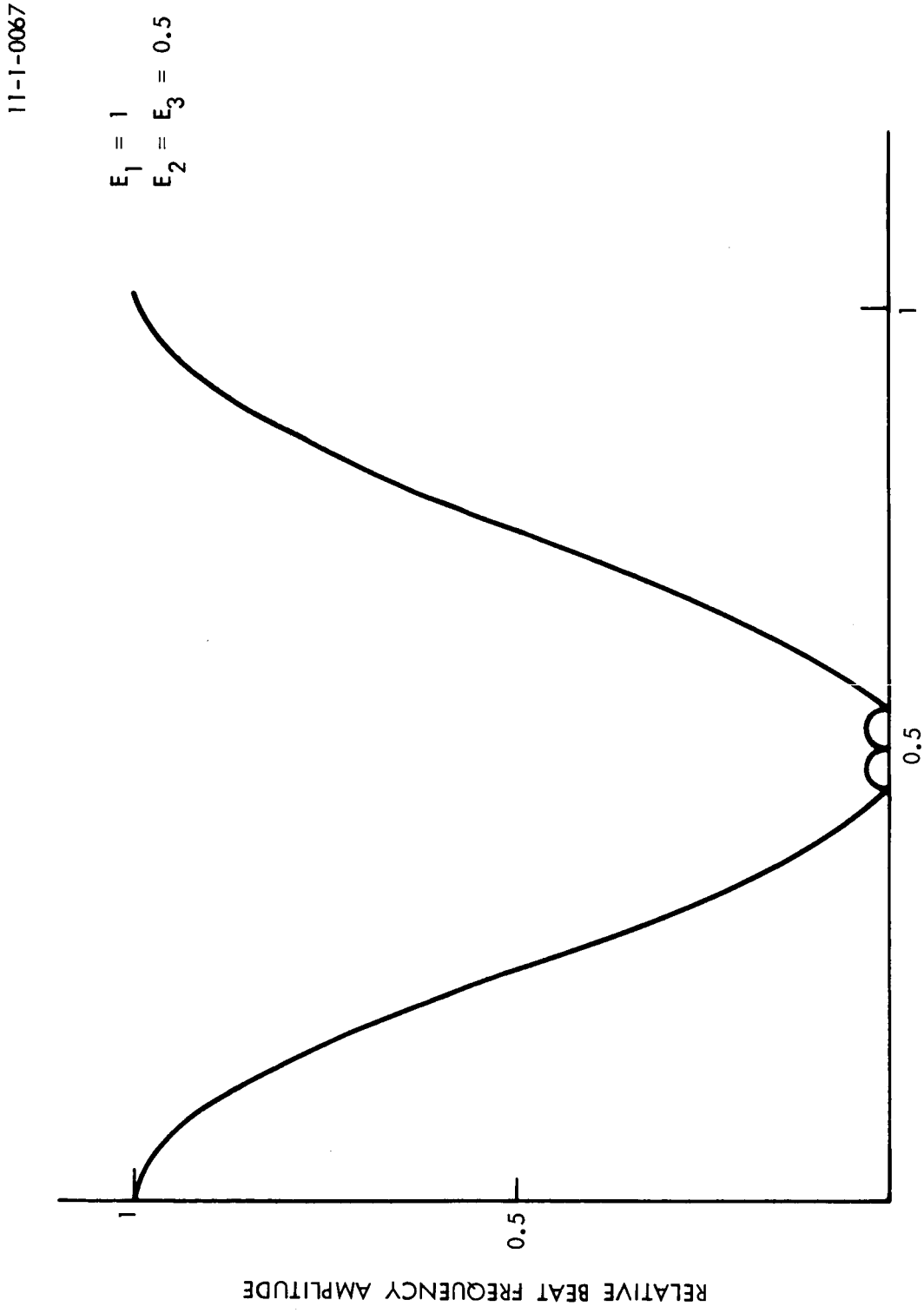

Figure B-3. Amplitude versus Range Curve.

APPENDIX C

ON MEASUREMENT OF THE DOPPLER SHIFT WITH LASERS

One of the big advantages of using lasers for tracking purposes is the high accuracy which can be obtained. As an example a laser emitting at the 6328 Å wavelength will display a doppler shift of approximately 1 Mc from a target moving at 1 ft/s. Some difficulty arises in practice from the fact that present day lasers do not emit only a single frequency, therefore the doppler shift is conveyed via several carriers simultaneously. It is essential to recognize the various frequency components present and discriminate the desired signal from them.

We begin by an analysis of the doppler effect where only one frequency is transmitted. The signal reflected from a moving target and received at the time t originated from the transmitter at the time $t-2\Delta t$. The instantaneous distance between the target and the transmitter-receiver is (see Figure C-1)

$$R(t) = R_o \pm v_r(t-t_o) \tag{C.1}$$

for $t > t_o$, and the range at time $t - \Delta t$ is:

$$R(t - \Delta t) = c\Delta t \ .$$

From which the delay time Δt can be found

$$R_o \pm v_r(t - \Delta t - t_o) = c\Delta t \ , \ \Delta t = \frac{R_o \pm v_r(t - t_o)}{c \pm v_r} \tag{C.2}$$

(+) sign is for a receding target

(-) sign is for an approaching target.

The received signal at the time t is then:

$$\sin\left[\omega_o(t-2\Delta t) + \phi\right] = \sin\left[\omega_o\left(t-2\,\frac{R_o \pm v_r(t- t_o)}{c \pm v_r}\right) + \phi\right] \ . \tag{C.3}$$

11-1-0068

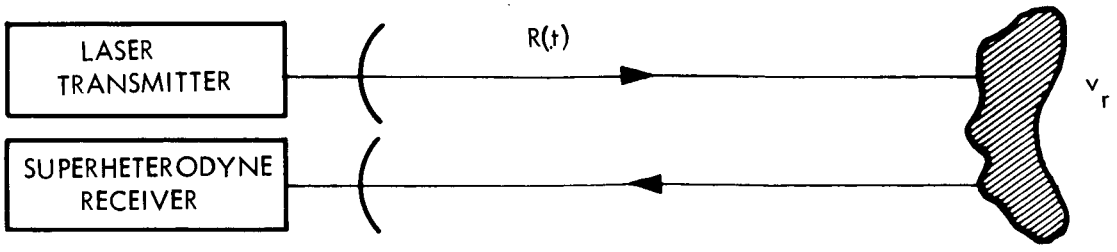

Figure C-1. A Doppler Laser System.

11-1-0070

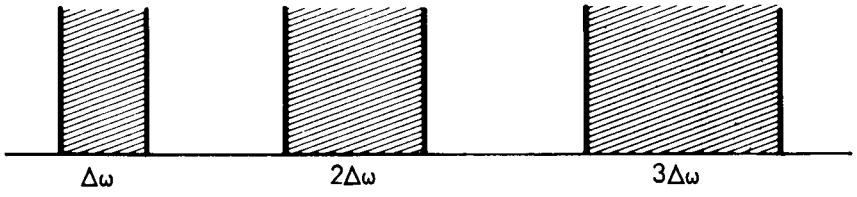

Figure C-2. Spectrum of Subcarrier Doppler Terms.

11-1-0069

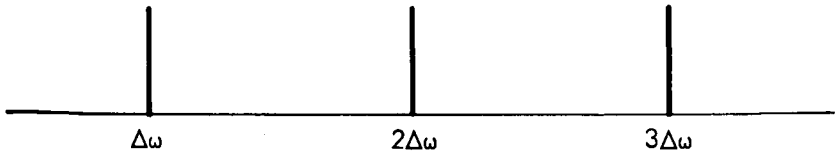

Figure C-3. Spectrum of Laser Beats.

In practice $\frac{v_r}{c} \ll 1$, so that we can expand

$$\left(1 \pm \frac{v_r}{c}\right)^{-1} = 1 \mp \frac{v_r}{c} \pm \frac{v_r^2}{c^2} + \cdots$$

Substituting into (C.3) and neglecting the higher powers of $\frac{v_r}{c}$ we have

$$\sin\left[\omega_o\left(t - 2\,\frac{R_o \pm v_r(t - t_o)}{c \pm v_r}\right) + \phi\right]$$

$$= \sin\left[\omega_o\left(t \mp \frac{2v_r}{c}\,t\right) - \frac{2\omega_o R_o}{c} + \frac{2\omega_o v_r t_o}{c} + \phi\right].$$

If we denote the doppler frequency by

$$\omega_D = 2\omega_o \frac{v_r}{c}$$

the received signal can be written

$$E_r(t) = A \sin\left[\left(\omega_o \mp \omega_D\right)t \pm \omega_D t_o - \frac{2\omega_o R_o}{c} + \phi\right]. \qquad (C.4)$$

In the superheterodyne receiver the signal is mixed with part of the transmitted signal and as a result a signal at the doppler frequency is obtained. If the local oscillator signal is written

$$E_\ell = A_\ell \sin\left(\omega_o t + \phi\right) \qquad (C.5)$$

the doppler signal is

$$E_{Dop} = \alpha\sqrt{AA_\ell}\cos\left(\omega_D t - \omega_D t_o \pm \frac{2\omega_o R_c}{c}\right). \qquad (C.6)$$

We now consider the more general case when a number of equally spaced frequencies are transmitted simultaneously. The transmitted signal takes the form:

$$\mathcal{E}(t) = \mathcal{E}_o \sin\left(\omega_o t+\phi_o\right) + \mathcal{E}_1 \sin\left(\omega_1 t+\phi_1\right) + \cdots \mathcal{E}_k \sin\left(\omega_k t+\phi_k\right) . \tag{C.7}$$

The received signal is given by:

$$E(t) = E_o \sin\left[\left(\omega_o \mp \omega_{Do}\right)t \pm \omega_{Do} t_o - 2\frac{\omega_o R_o}{c} + \phi_o\right]$$

$$+ \cdots E_k \sin\left[\left(\omega_k \mp \omega_{Dk}\right)t \pm \omega_{Dk} t_o - \frac{2\omega_k R_o}{c} + \phi_k\right] \tag{C.8}$$

where $\omega_k = \omega_o + k\Delta\omega$ with $\Delta\omega$ a fixed frequency separation and

$k = 0, \pm 1, \cdots, \pm n$ is an integer

$$\omega_{Dk} = \omega_k \frac{2v_r}{c} .$$

The received signal is mixed with part of the laser output, and the detector output is proportional to the incident power.

$$I_{Det} \propto \left\{\sum_k E_k \sin\left[\left(\omega_k \mp \omega_{Dk}\right)t \pm \omega_{Dk} t_o - \frac{2\omega_k R_o}{c} + \phi_k\right]\right.$$

$$\left. + \sum_k E'_k \sin\left(\omega_k t + \phi_k\right)\right\}^2 . \tag{C.9}$$

The mixing terms are given by:

$$\sum_{\substack{k,j \\ k\neq j}} \sqrt{E_k E_j} \sin\left[\left(\omega_k \mp \omega_{Dk}\right)t \pm \omega_{Dk} t_o - \frac{2\omega_k R_o}{c} + \phi_k\right]$$

$$\cdot \sin\left[\left(\omega_j \mp \omega_{Dj}\right)t \pm \omega_{Dj} t_o - \frac{2\omega_j R_o}{c} + \phi_j\right] \tag{C.10a}$$

$$\sum_{k,j}\sqrt{E_k E_j'}\ \sin\left[\left(\omega_k \mp \omega_{Dk}\right)t \pm \omega_{Dk}t_o - \frac{2\omega_k R_o}{c} + \phi_k\right] \cdot \sin\ \omega_j t+\phi_j$$

(C.10b)

$$\sum_{\substack{k,j \\ k\neq j}}\sqrt{E_k' E_j'}\ \sin\left(\omega_k t+\phi_k\right)\sin\left(\omega_j t+\phi_j\right) \quad . \tag{C.10c}$$

We will now analyze in detail the frequencies present in the various mixing terms. From the sum (C.10a) we obtain frequencies of the type;

$$\left(\omega_k - \omega_j\right)\mp\left(\omega_{Dk} - \omega_{Dj}\right) = (k - j)\ \Delta\omega\left(1 \mp \frac{2v_r}{c}\right) \quad .$$

These terms represent the laser beats with itself modulated by the doppler shift. They can be called therefore subcarrier doppler terms. Depending also on the velocity of the target they represent a relatively narrow spectrum centered around the beat frequencies as shown in Figure C-2. The width of the spectrum is proportional to the center frequency $(k-j)\Delta\omega$. From the sum (C.10c) we obtain terms at the frequencies

$$\omega_k - \omega_j = (k-j)\Delta\omega \quad .$$

This is a line spectrum and represents the beats of the laser local oscillator with itself. The spectrum is shown in Figure C-3. Finally we turn our attention to the sum (C.10b), this contains the terms which display the the doppler shift at the carrier frequency. The frequencies present are of the type:

$$\left|\left(\omega_k - \omega_j\right)\mp\ \omega_{Dk}\right| = \left|(k - j)\Delta\omega \mp \left(\omega_o+k\Delta\omega\right)\frac{2v_r}{c}\right| = \omega_{Do}+(k-j)\Delta\omega + k\Delta\omega\ \frac{2v_r}{c} \quad .$$

In particular we are interested only in the terms at the doppler frequency ω_{Do} or at approximately that frequency. These terms are obtained from the sum (C.10b) when we take k = j. The signal at the doppler frequency is then given by

$$A_{Dop}(t) = \sum_{k=-n}^{+n} A_k \cos\left(\omega_{Do} t + k\Delta\omega \frac{2v}{c} t + \psi_k\right) \qquad (C.11)$$

where

$$\psi_k = - \omega_{Dk} t_o \pm \frac{2\omega_k R_o}{c} \quad .$$

The expression for $A_{Dop}(t)$ can be expanded in the form:

$$A_{Dop}(t) = \cos \omega_{Do} t \sum_k A_k \cos\left(k\Delta\omega \frac{2v_r}{c} t + \psi_k\right)$$

$$- \sin \omega_{Do} t \sum_k A_k \sin\left(k\Delta\omega \frac{2v_r}{c} t + \psi_k\right) \quad . \qquad (C.12)$$

We now define:

$$A^2(t) = \left[\sum_k A_k \cos\left(k\Delta\omega \frac{2v}{c} t + \psi_k\right)\right]^2$$

$$+ \left[\sum_k A_k \sin\left(k\Delta\omega \frac{2v}{c} t + \psi_k\right)\right]^2 \qquad (C.13)$$

and

$$\tan \Phi(t) = \frac{\sum_{k=-n}^{n} A_k \sin\left(k\Delta\omega \frac{2v_r}{c} t + \psi_k\right)}{\sum_{k=-n}^{n} A_k \cos\left(k\Delta\omega \frac{2v_r}{c} t + \psi_k\right)} \quad . \qquad (C.14)$$

Thus:

$$A_{Dop}(t) = A(t)\cos\left[\omega_D t + \phi(t)\right] \quad . \tag{C.15}$$

From expression (C.15), we conclude that the doppler signal is both amplitude and frequency modulated. We can find the amplitude modulation envelope from the expression of A(t) which we rewrite in the form

$$A^2(t) = \sum_{k^2} A_k^2 + \sum_{\substack{k\ j \\ k\neq j}}\sum A_k A_j \cos\left[\mp(k-j)\Delta\omega\,\frac{2v_r}{c}\,t + \psi_k - \psi_j\right]$$

$$= \sum_k A_k^2 + \sum_k\sum_j A_k A_j \cos\left[\frac{2(k-j)\Delta\omega}{c}\left[R_o \pm v_r\left(t - t_o\right)\right]\right] \tag{C.16}$$

if we now denote:

$$\frac{c}{\Delta\omega} = \frac{\Delta\lambda}{2\pi}$$

and use the expression for R(t) we obtain

$$A^2(t) = \sum_{k=-n}^{n} A_k^2 + \sum_{\substack{k=-n\,j=-n \\ k\neq j}}^{n}\sum^{n} A_k A_j \cos\frac{2\pi(k-j)}{\frac{\Delta\lambda}{2}}\,R(t) \quad . \tag{C.17}$$

This final expression (C.17) is analogous to the spatial distribution pattern obtained from a stationary target (see Equation (B.9) in Appendix B). Thus the envelope of the amplitude modulated doppler return signal is just the spatial distribution pattern moving at a velocity v_r along the direction of propagation.

We can find the amount of frequency modulation present by taking the derivative of (C.14)

$$\omega_m = \frac{d\phi}{dt} = \frac{1}{1 + \tan^2\phi t} \frac{\sum_{k=-n}^{n} \sum_{j=-n}^{n} k\Delta\omega \frac{2v_r}{c} A_k A_j \cos\left[(k-j)\Delta\omega \frac{2v_r}{c} t + \psi_k - \psi_j\right]}{\left[\sum_{k=-n}^{n} A_k \cos\left(k\Delta\omega \frac{2v_r}{c} t + \psi_k\right)\right]^2}$$

$$\omega_m = \frac{\sum_{k=-n}^{n} \sum_{j=-n}^{n} k\Delta\omega_D A_k A_j \cos 2\pi(k-j)\frac{R(t)}{\frac{\Delta\lambda}{2}}}{\sum_{k=-n}^{n} A_k^2 + \sum_{\substack{k=-n \\ k\neq j}}^{n} \sum_{j=-n}^{n} A_k A_j \cos 2\pi(k-j)\frac{R(t)}{\frac{\Delta\lambda}{2}}}$$

where

$$\Delta\omega_D = \Delta\omega \frac{2v_r}{c} .$$

Alternatively we can write

$$\omega_m = \Delta\omega_D \frac{\sum_{k=1}^{n} \sum_{j=1}^{n} k\left\{\left(A_k A_j - A_{-k} A_{-j}\right)\cos 2\pi(k-j)\frac{R(t)}{\frac{\Delta\lambda}{2}} + \left(A_k A_{-j} - A_{-k} A_j\right)\cos 2\pi(k+j)\frac{R(t)}{\frac{\Delta\lambda}{2}}\right\}}{A_o^2 + \sum_{k=1}^{n}\left(A_k^2 + A_{-k}^2\right) + \sum_{k=1}^{n}\sum_{j=1}^{n}\left\{\left(A_k A_j + A_{-k} A_{-j}\right)\cos 2\pi(k-j)\frac{R(t)}{\frac{\Delta\lambda}{2}} + \left(A_k A_{-j} + A_{-k} A_j\right)\cos 2\pi(k+j)\frac{R(t)}{\frac{\Delta\lambda}{2}}\right\}}$$

(C.18)

In this latter form it is apparent that ω_m vanishes for all times provided we make $A_k = A_{-k}$, that is if the energy of the laser is symmetrically distributed about the main frequency. We can also put in evidence the various frequency components in ω_m by writing

$$\omega_m = \Delta\omega_D \frac{\sum_{m=1}^{n} b_m \cos 2\pi \frac{mR(t)}{\frac{\Delta\lambda}{2}}}{1 + a_o + \sum_{m=1}^{2n} a_m \cos 2\pi \frac{mR(t)}{\frac{\Delta\lambda}{2}}} \qquad (C.19)$$

where

$$a_m = \sum_{j=-n}^{n} \frac{A_j}{A_o}\left(\frac{A_{j+m}}{A_o} + \frac{A_{j-m}}{A_o}\right) \qquad \text{for } m \neq 0$$

$$a_o = \sum_{j=1}^{n}\left(\frac{A_j^2}{A_o^2} + \frac{A_{-j}^2}{A_o^2}\right) \qquad \text{for } m = 0$$

$$b_m = \sum_{j=-n}^{n} j \frac{A_i}{A_o}\left(\frac{A_{j+m}}{A_o} + \frac{A_{j-m}}{A_o}\right) .$$

The maximum of ω_m occurs for $\frac{\partial \omega_m}{\partial t} = 0$. This can be found as follows. Let ω_m be written as:

$$\omega_m = \frac{f(t)}{g(t)}$$

$$\frac{\partial \omega_m}{\partial t} = \frac{f'(t)g(t) - f(t)g'(t)}{g^2(t)} .$$

At a maximum we have:

$$\frac{f'(\tau)}{g'(\tau)} = \frac{f(\tau)}{g(\tau)}$$

which then determines the time τ. Thus:

$$\left(\omega_m\right)_{max} = \Delta\omega_D \frac{\sum_m m b_m \sin 2\pi \frac{mR(\tau)}{\frac{\Delta\lambda}{2}}}{\sum_m m a_m \sin 2\pi \frac{mR(\tau)}{\frac{\Delta\lambda}{2}}} \quad . \tag{C.20}$$

If the amplitudes of the higher order side-frequencies emitted by the laser decrease sufficiently rapidly it can be also shown that $a_m > b_m$. Therefore we conclude that $\left(\omega_m\right)_{max} \leq \Delta\omega_D$; this sets a bound on the frequency excursion due to frequency modulation.

APPENDIX D

NOISE FIGURE FOR PHOTOTUBES

The signal-to-noise ratio P_{so}/P_{no} for photon noise limited operation is given by the equation*

$$\frac{P_{so}}{P_{no}} = \frac{QP_s}{h\nu\Delta f} \tag{D.1}$$

where

Q = quantum efficiency
P_s = signal power
$h\nu$ = energy per photon
Δf = electrical bandwidth.

The noise equivalent power, P_N, is defined as the amount of signal power required to give a unity signal-to-noise ratio. Thus from Eq. (D.1)

$$P_N = \frac{h\nu\Delta f}{Q} \quad . \tag{D.2}$$

The maximum sensitivity will be obtained when $Q = 1$. Thus the noise figure reference power is

$$(P_N)_{Q=1} = h\nu\Delta f \quad . \tag{D.3}$$

The noise figure F_{opt} for an optical superheterodyne receiver may be defined as the ratio of the noise equivalent power of the receiver P_N to the value $(P_N)_{Q=1}$. Expressing this mathematically results in

$$F_{opt} = \frac{P_N}{(P_N)_{Q=1}} = \frac{P_N}{h\nu\Delta f} \quad . \tag{D.4}$$

Equation 56 of Biernson and Lucy* is

*Biernson G., and Lucy R.F., "Requirements of a Coherent Laser Pulse Doppler Radar," Proc. IEEE, Vol. 51, Jan. 1963, pp. 202-213.

$$\frac{P_{so}}{P_{no}} = \frac{QP_s}{h\nu\Delta f\left[1 + \frac{P_n}{P_r} + \left[\frac{FkTh\nu}{2RG^2Qe^2}\right]\frac{1}{P_r} + 2Q\Sigma p_n\right]} \tag{D.5}$$

where the terms not previously defined are

P_n = total equivalent power due to radiation background, dark current, etc.

P_r = local oscillator power

FkT = noise energy of amplifier following phototube

R = effective load resistance of phototube

G = phototube gain

e = electron charge

$2Q\Sigma p_n$ = normalized beat term due to local oscillator beating with background power.

For diffuse solar background and a local oscillator power greater than

$$\frac{P_n}{P_r} << 1 \tag{D.6}$$

$$2Q\Sigma p_n << 1 \, . \tag{D.7}$$

Equation (D.5) becomes

$$\frac{P_{so}}{P_{no}} = \frac{QP_s}{h\nu\Delta f\left[1 + \frac{FkTh\nu}{2RG^2Qe^2P_r}\right]} \tag{D.8}$$

when

$$\frac{P_{so}}{P_{no}} = 1 \tag{D.9}$$

$$P_s = P_N \quad . \tag{D.10}$$

Substituting and then solving for P_N we get

$$P_N = \frac{h\nu\Delta f}{Q}\left[1 + \frac{FkTh\nu}{2RG^2Qe^2P_r}\right] \quad . \tag{D.11}$$

Substituting in Eq. (D.4) the optical noise figure is

$$F_{opt} = \frac{1}{Q}\left[1 + \frac{FkTh\nu}{2RG^2Qe^2P_r}\right] \quad . \tag{D.12}$$

APPENDIX E

SPATIAL TRACKER SERVO CONTROL DESIGN

1. MISSION, GENERAL CONFIGURATION, AND TARGET MOTION INDUCED ERRORS

The tracker-target geometric configuration is shown in Figure E-1.

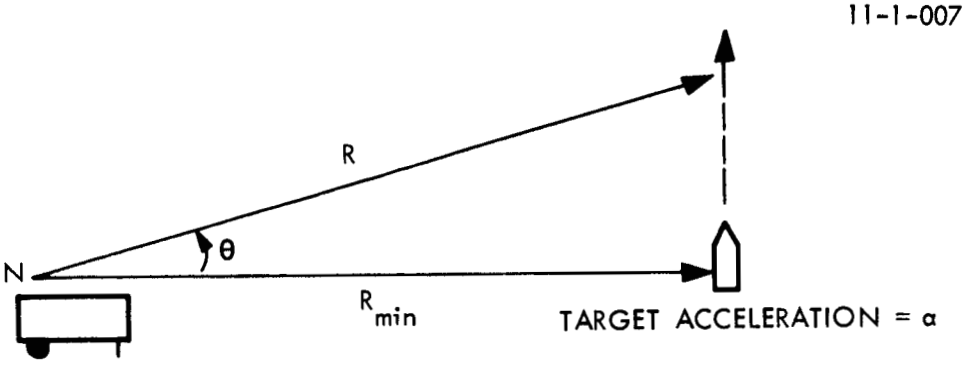

Figure E-1. Postulated Operational Environment.

From considerations of this geometry the maximum angle velocity, $\dot{\theta}_{max}$, is

$$\dot{\theta}_{max} = 0.8\left(\frac{\alpha}{R_{min}}\right)^{\frac{1}{2}}$$

while the maximum angular acceleration, $\ddot{\theta}_{max}$, occurs at launch and equals

$$\ddot{\theta}_{max} = \frac{\alpha}{R_{min}}$$

where

α target acceleration [ft/sec^2]

R_{min} distance from tracker to launch position.

The block diagram of the control loop is shown in Figure E-2. The resonance of the controlled structure will be assumed to be 100 c/s. If the rate loop bandwidth is thus limited, the following rate loop parameters are appropriate.

rate loop gain-cross-over freq.	$\omega_r = 150$ 1/s	Not necessarily used.
rate loop integ. network upper break freq.	$\omega_{ir} = 50$ 1/s	
ratio of rate loop integ. net. break frequencies	$\beta = 50$	

The character of the noise at the detector is difficult to estimate but noise bandwidth associated with the following position loop parameters is assumed for the present to provide adequate filtering.

position loop gain-cross-over freq.	$\omega_p = 30$ 1/s
position loop integ. network upper break frequency	$\omega_{ip} = 10$ 1/s
ratio of pos. loop integ. net. break frequencies	$\alpha = 100$

The gain-cross-over of a control loop is analogous to the loop bandwidth and is more strictly defined as the frequency at which the open-loop gain transfer function equals unity. Any integral networks included in the loop must have upper break frequencies at less than the gain-cross-over frequency for stability reasons. If the target acceleration is taken as 100 ft/s^2 and the minimum range as 5,000 ft, the angular error due to an input at the max angular velocity would be

$$\theta_{e(v)} = \frac{0.8\left(\frac{\alpha}{R_{min}}\right)^{\frac{1}{2}}}{\omega_p \alpha} = \frac{0.11}{(30)(100)} = 0.038 \text{ milliradian} .$$

The corresponding tracking error due to an input at the maximum angular acceleration is

11-1-0072

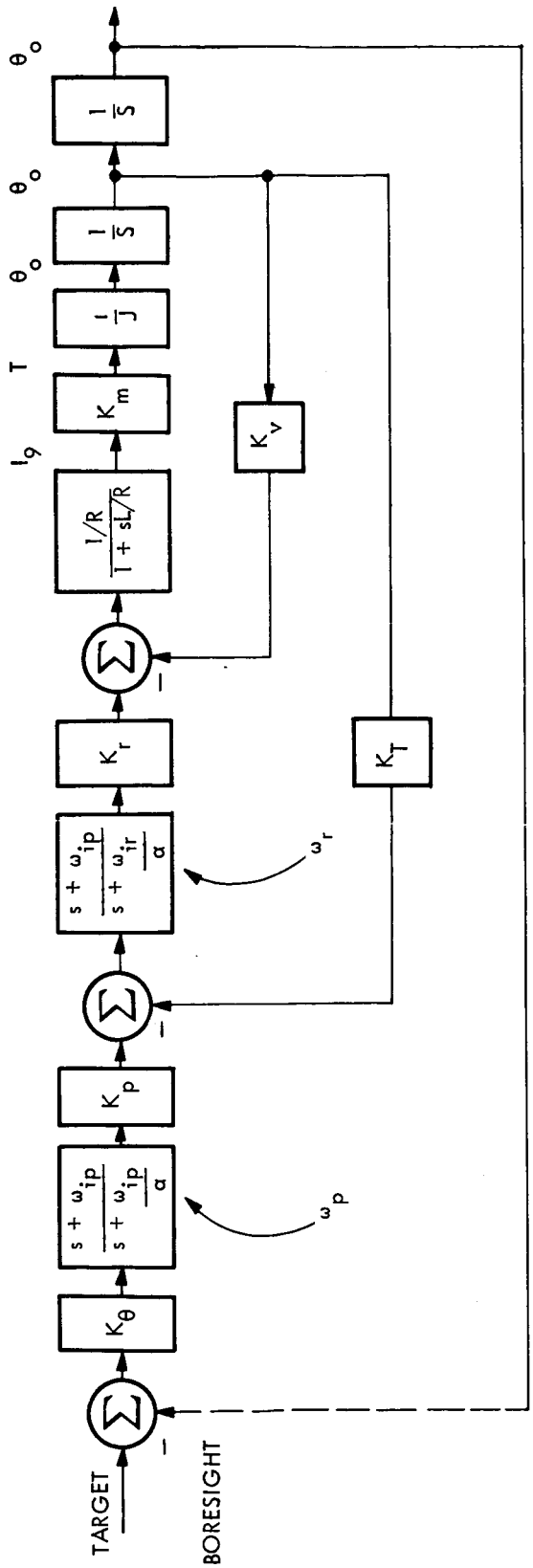

Figure E-2. Block Diagram of Control Loop.

$$\theta_{e(a)} = \frac{\alpha/R_{min}}{\omega_p \omega_{ip}} = \frac{100/5000}{(30)(10)} = 0.067 \text{ milliradian} .$$

These two errors are less than the desired tracking accuracy of 0.1 milliradians.

2. PARTICULAR COMPONENTS

The total load inertia including motor is estimated at $J_T = 1.0$ ft-lb-sec^2 and for this value and the maximum acceleration the stall torque required is

$$T_p = J_T \ddot{\theta}_{max} = 1(0.12) = 0.02 \text{ ft lb} .$$

The motor torque requirement however is set by the required step-response which indicates that for no overshoots, the necessary torque would be

$$T = \frac{J \dot{\theta}_{max} \omega_c}{2} = \frac{(1.0)(0.1)(30)}{2} = 1.5 \text{ lb-ft} .$$

This indicated an Inland T-4036 capable of 1.8 lb-ft stall torque and 37 rad/s max no-load speed. The electrical time constant

$$\tau_E = L/R = 2 \times 10^{-3} \text{sec} .$$

For a 4 ohm armature resistance an inductance of 8×10^{-3} Henry is indicated. The motor is to be driven by a solid state power amplifier with an output impedance of 2 ohm estimated. The total armature circuit resistance is then 6 ohms. The armature transfer function is then

$$Y_a = \frac{1}{R+SL} = \frac{1/R}{1+SL/R} = \frac{1/6}{1 + S/650} .$$

The open motor loop transfer function is then

$$G_m = \frac{K_m K_v}{RJS(1+S/650)} .$$

For the T-4036 with a 4 ohm armature resistance the motor constant $K_m = 0.378$ lb-ft/A. The back emf of any torque motor is 1.356 times the motor constant so $K_v = 1.356_m$ and

$$G_m = \frac{(0.378)^2(1.356)}{(6)(1)S(1+S/650)} = \frac{0.032}{S(1+S/650)} .$$

The closed motor loop transfer function is then

$$\frac{G_m}{1+G_m} = \frac{0.032}{(S+0.032)(1+S/650)}$$

which is shown as the open-loop rate transfer function on Figure E-3. The open loop rate transfer function is (neglecting net)

$$G_r = \frac{K_r K_t}{K_v} \frac{0.032}{(S+0.032)(1+S/650)} .$$

Hence for a gain-cross-over frequency of 150 1/s

$$\frac{K_r K_t}{K_v} = \frac{150}{0.032} = 4700 .$$

The preliminary tachometer selection indicated of the the Inland T-5703 as a reasonable rate feedback element. This unit has a sensitivity of 32 volts/rad/s and a maximum ripple of 1% of the average most of which occurs at a frequency of 79 ripple cycles/rev. Thus the rate loop amplifier K_r must have a gain equal to

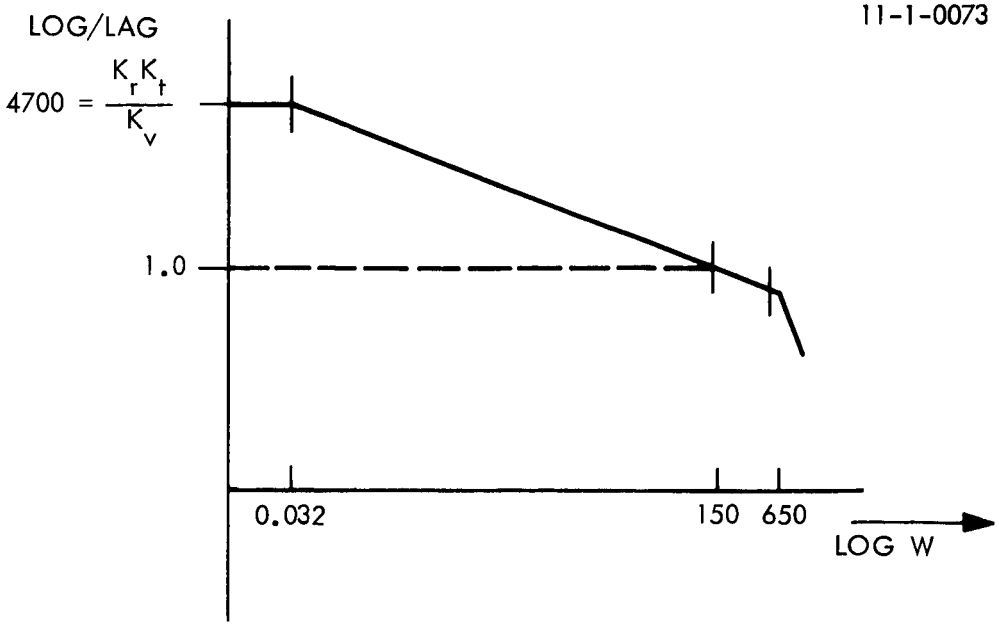

Figure E-3. Log Magnitude Plot of Rate Loop Gain Transfer Function.

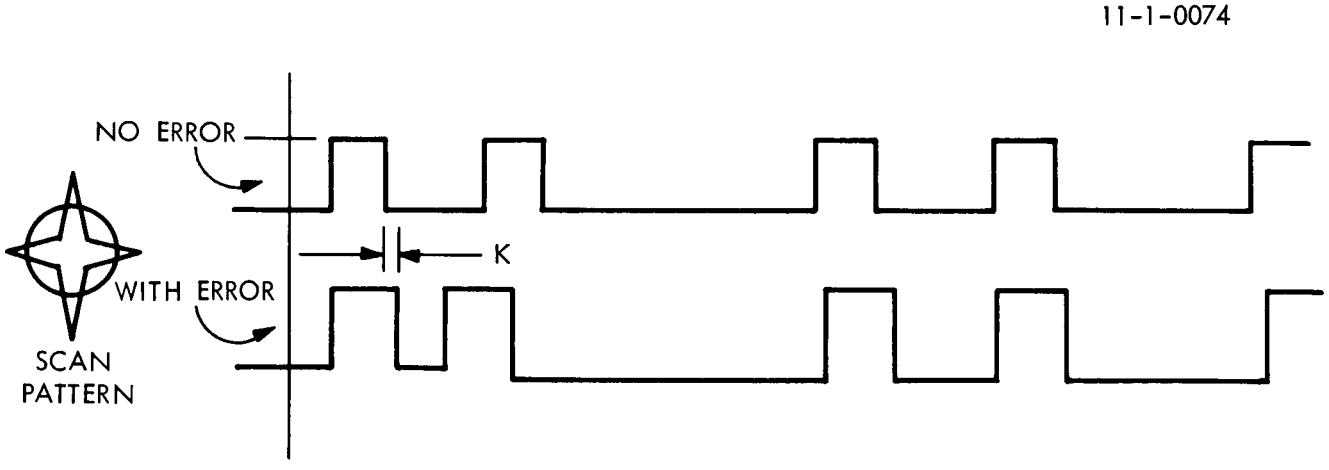

Figure E-4. Image Dissector Output Waveforms with Star Scan Pattern as Indicated.

$$K_r = 4700 \frac{K_v}{K_t} = 4700 \frac{0.514}{32} = 75 \ .$$

For the position loop the open loop transfer function again neglecting the integral networks is

$$\frac{K_p K_\theta}{K_t S} = G_p$$

and for $\omega_p = 30$ 1/s

$$K_p K_\theta = 30 K_t = (30)(30) = 900 \ .$$

For the position loop, the analysis of a ITT Star Tracker electronically scanned photomultiplier with aperture whose output waveform is shown in Figure E-4 gives the result that the magnitude of the fundamental component which is absent for no error is equal to

$$a_1 = \frac{2A}{\pi} (0.92)(6.28)K = 36.8K$$

where K denotes the amount of the scan represented by the deviation from the no error condition, $0 \leq K$ C 1/16, if the aperture is 3 milliradians in extent, for one milliradian movement from center

$$k = \left(\frac{1}{1.5}\right)\left(\frac{1}{16}\right) = 0.0416 \ .$$

Thus if we make $K_p = 1$, $K_\theta = 900$

$$a_1 = \frac{2A}{\pi} (0.92)(6.28)(0.0416)\left[\frac{\text{volts}}{\text{millirad}}\right]$$

$$K_\theta = 900\left[\frac{\text{volt}}{\text{rad}}\right] = 0.9\left[\frac{\text{volts}}{\text{millirad}}\right] \ .$$

Thus,

$$a_1 = K_\theta$$

$$A = \frac{0.9}{4(0.92)(0.0416)} = 4.85 \text{ volts.}$$

Thus clamping the output voltage of the square wave at 4.85 volts produces an error signal at the necessary $900\left[\frac{\text{volt}}{\text{rad}}\right]$ with the scan pattern shown.

3. SYSTEM ERRORS DUE TO NOISE, STICTION, AND EXTERNAL TORQUES

The tracking errors due to target motion were considered first and used to set various parameter values. However there remains to consider the errors due to such sources as tachometer noise and stiction or external torques.

Basically the error due to tachometer noise is

$$\theta_{e(t)} = \frac{(0.01)(0.1)}{\omega_c} = \frac{0.001}{30} = 0.033 \text{ milliradian .}$$

The rate at which this signal occurs is

$$70[\text{c/rev}] \times 6.28[\text{rad/c}] \times 0.1[\text{rad/s}] \times 1/6.28[\text{rev/rad}] = 7.9[\text{rad/s}]$$

which is seen to be only slightly below the upper break frequency of the integral networks; hence, it will not be much affected by it. However all lower frequency ripple components corresponding to lower input angular rates will cause errors of less magnitude because of the integral network. Finally since all the expected ripple frequencies fall well within the position loop bandwidth there should be no saturation problem in the rate loop because of the ripple voltage since the position loop can respond fast enough to make the effective rate loop ripple input equal zero.

The maximum error due to a load torque introduced into a system with a rate loop integral network with a break frequency greater than up can be expressed as

$$\theta_{e(t_L)} = \frac{T_L}{J\omega_r\omega_{ir}}$$

so for

$$\theta_e = 0.03 \text{ [mils]}$$

$$T_L = (3 \times 10^{-5})(1)(50)(150)$$

$$= 0.225 \text{ [ft-lb]}$$

$$= 43.4 \text{ [oz-in]} .$$

The stiction torque of the T-5703 = 15 (oz-in) and the T-4036 has 6.8 (oz-in) for a total of approximately 22(oz-in). Since the expected load torques due to wind will be very small, the rate loop integral network may not be necessary in which case the allowable torque would be

$$T_L = (\theta_e)J\omega_r\omega_p$$

$$= 26 \text{ [oz-in]} .$$

4. INPUT NOISE

The noise level at the input of the integral network should be less than the voltage corresponding to 0.01 milliradian which corresponds to 9 millivolts as seen from the image dissector transfer function of $900\left[\frac{\text{volts}}{\text{rad}}\right]$.